Role of mTOR in autophagic and lysosomal reactions to environmental stressors in molluscs

Susanna Sforzini [a,b], Michael N. Moore [a, c, d, e], Caterina Oliveri [a], Anna Volta [a], Awadhesh Jha [e], Mohamed Banni [a, f], Aldo Viarengo [a, b]

[a] Department of Sciences and Technological Innovation (DiSIT), University of Piemonte Orientale "A. Avogadro", V.le T. Michel 11, 15121 Alessandria, Italy

[b] Laboratory of Environmental Chemistry and Toxicology, IRCCS - Istituto di Ricerche Farmacologiche Mario Negri, Via Giuseppe La Masa 19, 20156 Milan, Italy

[c] European Centre for Environment & Human Health (ECEHH), University of Exeter Medical School, Truro, TR1 3HD, UK

[d] Plymouth Marine Laboratory, Plymouth, PL1 3DH, UK

[e] School of Biological and Marine Sciences, University of Plymouth, Drake Circus, Plymouth, PL4 8AA, UK

[f] Laboratory of Biochemistry and Environmental Toxicology, ISA, Chott-Mariem, Sousse, Tunisia

Corresponding author:

Aldo Viarengo

Department of Sciences and Technological Innovation (DiSIT), University of Piemonte Orientale "A. Avogadro", V.le T. Michel 11, 15121 Alessandria, Italy

Phone: + 390131360370

Fax: +390131360390

e-mail: viarengo@uniupo.it

Abstract

Lysosomal membrane stability (LMS) has been used in various organisms as a very sensitive biomarker of stress. However, despite the abundance of data about regulation of the autophagic process in mammals, in the invertebrates there is only limited mechanistic understanding. Marine mussels (*Mytilus galloprovincialis* Lam.) are bivalve molluscs, widely used as models in ecotoxicology and as environmental bioindicators of sea water quality. In order to elucidate this fundamental process, in the present study, mussels were exposed for 3 days to a "priority", ubiquitous environmental contaminant, benzo[*a*]pyrene (B[*a*]P) at different concentrations (i.e. 5, 50, 100 µg/L seawater). B[*a*]P accumulated in lysosomes of digestive tubule epithelial cells (digestive cells) and in enlarged lipid-rich lysosomes (autolysosomes) as detected by immunofluorescence and UV-fluorescence. B[*a*]P also activated the autophagic process with a marked decrease of LMS and concurrent increase in lysosomal/cytoplasmic volume ratio. Dephosphorylation of mTOR contributes to increased lysosomal membrane permeability and induced autophagy. B[*a*]P induced a decrease in phosphorylated (active form) mTOR. The probable role of mTOR in cell signalling and the regulation of the cellular responses to the contaminants has been also confirmed in a field study, where there was significant inactivation of mTOR in stressed animals. Statistical and network modelling supported the empirical investigations of autophagy and mTOR; and was used to integrate the mechanistic biomarker data with chemical analysis and DNA damage.

Keywords: mussel, autophagy, B[*a*]P, mTOR, network modelling

1. Introduction

Over the last decades, the studies about the biological effects of environmental stressors including toxic chemicals have led to development of numerous biomarkers at different levels of functional complexity suitable to follow the evolution of the stress syndrome from the early warning signals at the molecular/cellular level to the deterioration at the organism level (Moore et al., 2012; Viarengo et al., 2007). Among others, numerous lysosomal-related biomarkers have been developed; lysosomes, highly conserved organelles playing a pivotal role in many cellular processes, were shown to be the target for a wide range of contaminants (Appelqvist et al., 2013; Moore, 1988; Moore et al., 2007; Viarengo and Nott, 1993). In particular, lysosomal membrane stability (LMS), whose reduction represents a subcellular pathological reaction known to be linked to augmented autophagic sequestration of cellular components, has been used both in invertebrates and vertebrates as a very sensitive and easy to use biomarker of stress (Fernández et al., 2005; Moore et al., 2004a; Sforzini et al., 2015; Svendsen et al., 2004).

Autophagy (i.e. macroautophagy), the major inducible pathway for general turnover of cytoplasmic components, takes place in all eukaryotic cells (Klionsky and Emr, 2000). This process plays an essential role in promoting cell survival in response to metabolic as well toxic stress by the sequestration of cytoplasmic components, the removal of damaged organelles and protein aggregates and their subsequent degradation in lysosomes. However, an excessive autophagic rate has been shown to have deleterious consequences for tissue/organism health (Levine and Kroemer, 2008). Autophagy is well documented in marine mussels using biochemical, cell fractionation, cytochemical and ultrastructural methods, where it is induced by many environmental stressors including fasting, increased salinity, polycyclic aromatic hydrocarbons (PAHs) and chloroquine (Bayne et al., 1980; Moore, 2004, 2008; Moore & Clarke, 1982; Moore et al., 1980, 1996, 2006a, b; 2007; Nott et al., 1985; Pipe & Moore, 1985).

Stress-induced autophagy, such as that induced by nutrient starvation, is regulated by the inhibition of mTOR (mechanistic Target of Rapamycin) in eukaryotic cells from yeast to mammals (Klionsky and Emr, 2000; Moore et al., 2012). mTOR is an evolutionarily-conserved serine/threonine protein kinase that senses and integrates a variety of cellular physiological and environmental signals to regulate cell growth (Jung et al., 2010). The phosphorylated active form of mTOR is involved in various processes, such as activation of protein translation (transcription, ribosome biogenesis, protein synthesis) and inhibition of the autophagic activity (Dowling et al., 2010; Soulard et al., 2009). Despite the large number of studies on mammals demonstrating the existence of multiple diverse regulators of mTOR and its involvement in the onset of several pathologies (Laplante and Sabatini, 2012), the research on TOR signalling in invertebrates and in particular in contaminant exposed organisms is an area where much remains to be explored (Soulard et al., 2009).

Molluscs are extensively used as models in many research fields (Abele et al., 2009; Gliński and Jarosz, 1997); and are widely employed (in particular *Mytilus* sp.) as sentinel organisms in biomonitoring programs (such as Med Pol, UNEP Mediterranean Biomonitoring Program; OSPAR Convention; RA.MO.GE.; UNIDO) (Viarengo et al., 2007). The aim of this work was to investigate the alterations of the lysosomal vacuolar system and the possible involvement of mTOR in their regulation in the digestive gland of mussels *M. galloprovincialis* Lam. exposed to benzo[*a*]pyrene (B[*a*]P), chosen as model organic xenobiotic. This toxic and genotoxic compound, priority pollutant listed by U.S. EPA (Environmental Protection Agency) (U.S. EPA, 2009), is ubiquitous in the environment and tends to persist and bioaccumulate through the food chain (Wang and Wang, 2006).

Following exposure to B[*a*]P, we investigated in mussel digestive gland (organ with storage and distribution function; Bayne, 2009) firstly the accumulation and the subcellular distribution of B[*a*]P, detected by immunofluorescence analysis using an anti-PAHs antibody. Moreover, in this tissue, the effects on LMS and lysosomal/cytoplasmic (L/C) volume ratio, able to highlight the level

of stress in the organisms, from the early warning cellular signals (i.e. increased lysosomal autophagic activity) to tissue pathology (i.e. excessive autophagy can trigger cell catabolism leading to a loss of tissue functionality) were also measured. As a possible key element involved in the regulation of the lysosomal activity, the role of the mTOR was evaluated by immunolabelling. The level of mTOR phosphorylation was also investigated in mussels sampled in field from areas at different levels of organic xenobiotic contamination.

Mathematical models provide the conceptual and mathematical formalism to integrate molecular, cellular and whole animal processes (Allen & McVeigh, 2004; Allen & Moore, 2004; Moore & Noble, 2004). Previous studies have shown that network complexity (as evaluated using network connectedness -connectance CV%- and node size) can be used as an indicator of homeostasis or health in cellular systems (Moore, 2010).

Modelling is essential for the derivation of explanatory frameworks that facilitates the development of a predictive capacity for estimating outcomes or risk associated with particular disease processes and stressful treatments (Moore, 2010; Moore & Noble, 2004; Moore et al., 2015). Previous studies on mussels and earthworms have shown that there is a strong relationship between lysosomal membrane stability (LMS), as an indicator of cellular health, and the responses of numerous stress biomarkers (Moore et al., 2006a; Sforzini et al., 2015, 2017). In this investigation, principal component analysis and network modelling was used to integrate multi-biomarker data; and to test a predictive complexity model of cellular patho-physiological function.

2. Materials and methods

2.1. Chemicals and organisms

All chemicals were of analytical grade and purchased from Sigma-Aldrich Co. (UK/Italy), unless otherwise indicated. Adult *Mytilus galloprovincialis* Lam. (50.7 ± 2.8 mm) were collected from the intertidal zone at Trebarwith Strand, Cornwall, UK (50° 38’ 40" N, 4° 45’ 44" W) in October 2014

(Banni et al, 2017). The site is relatively free of disease and is remotely located (Bignell et al., 2011). Mussels were transported back to the laboratory in cool boxes and allowed to depurate for 7 days in natural seawater from Plymouth Sound. The seawater was maintained at 15.3 ± 0.68 °C and filtered before to start the experiment (pH 7.9 ± 0.06). During the depuration period, mussels were fed with a suspension of *Isochrysis galbana* every 3 days (1.05×10^6 cells/mL), with a 100% water change 2 h after each feeding.

2.2. Experimental design and sampling

After depuration, the mussels were transferred to 2-L glass beakers containing 1.8 L of the same seawater as above and allowed to acclimatize for 48 h. The experiment began after this period and consisted of a 3-day static exposure with no water changes, during which the mussels were not fed. Two mussels were used per beaker. A photoperiod of 12 h light : 12 h dark was maintained throughout the experiment. Good seawater oxygenation was provided by a bubbling system. Seawater quality was monitored in each of the beakers by measuring salinity (35.4 ± 0.09‰), pH (7.9 ± 0.06), % dissolved oxygen (97.9 ± 3.22%) and temperature (15.3 ± 0.68 °C) (Banni et al., 2017). Groups of mussels were exposed to four treatments i.e. solvent control (0.02% dimethyl sulfoxide [DMSO]; 36 mussels); 5 μg/L B[*a*]P (36 mussels); 50 μg/L B[*a*]P (36 mussels); 100 μg/L B[*a*]P (36 mussels). After 3 days exposure period, digestive glands were rapidly removed, placed on aluminium cryostat chucks, chilled in super-cooled n-hexane and stored at -80 °C.

The B[a]P concentrations used in these experiments were selected taking into account that the levels of PAHs in the sea water of contaminated environment range from 0.26 μg/L (Manodori et al., 2006), 18.34 μg/L (Sinaei and Mashinchian, 2014) to 46 μg/L (Nasher et al., 2013). After 3 d of exposure, the amount of chemical in the tissues of exposed animals was similar to that detected in the tissues of mussels sampled in field contaminated coastal waters (Banni et al., 2017; Widdows et al., 2002).

147

148 *2.3. Lysosomal alterations*

149 Frozen digestive gland sections (10 μm) of mussels from each exposure condition were cut by
150 cryostat (LeicaCM3050) and flash-dried by transferring them onto slides at room temperature.
151 Lysosomal membrane stability: The determination of LMS in the cells of the digestive gland was
152 performed on cryostat tissue sections following essentially the method described by Moore (1988).
153 This cytochemical assay is based on acid labilization characteristics of latent hydrolase β-*N*-
154 acetylhexosaminidase (NAH) using naphthol AS-BI-N-acetyl-β-D glucosaminide as a substrate for
155 NAH. Slides were observed using an inverted microscope (Zeiss Axiovert 100M) at 400 ×
156 magnification, connected to a digital camera (Zeiss AxioCam). The pictures obtained were analysed
157 using an image analysis system (Scion Image) that allowed for the determination of the labilisation
158 period i.e. the incubation time in the acid buffer needed to produce the maximal lysosomal staining.
159 Lysosomal/cytoplasmic (L/C) volume ratio: the L/C volume ratio of the digestive gland tissue was
160 evaluated following the method described by Moore (1976) and Moore and Clarke (1982).
161 Lysosomes were reacted for the lysosomal enzyme β-*N*-acetylhexosaminidase (NAH) using
162 naphthol AS-BI-N-acetyl-β-D glucosaminide as a substrate for NAH. The ratio between
163 cytoplasmic and lysosomal volumes was determined by analysing the images obtained from the
164 slides at 400 × magnification by image analysis as described above and expressed as a percentage
165 variation with respect to controls.

166

167 *2.4. Immunofluorescence analysis*

168 Cryostat frozen digestive gland sections (10 μm) obtained as described above were flash-dried by
169 transferring them onto poly-L-lysine-coated microscope slides at room temperature and fixed in
170 paraformaldehyde (PFA) solution (4% PFA in phosphate buffer saline-PBS, pH 7.2, 20 min at 20 ±
171 1 °C).

Immunofluorescent anti-PAHs staining was carried out as described by Sforzini et al., 2014. Briefly, after fixation, sections were washed three times in PBS (5 min) and incubated in a permeabilisation and blocking solution (0.5% Triton X-100, 2% bovine serum albumin-BSA, 0.5% rabbit serum in PBS) for 1 h at 20 ± 1 °C. After rinsing, sections were incubated with the primary antibody (monoclonal mouse anti-PAHs, Santa Cruz Biotechnology Inc., 1/100 in PBS containing 1% BSA and 0.05% Triton X-100) overnight at 4 °C in a moist chamber. Then, the sections were washed (three times in PBS, 5 min) and the secondary antibody was applied i.e. polyclonal rabbit to mouse IgG (FITC) (Abcam) (1/100 in 1% BSA and 0.05% Triton X-100 in PBS) for 1 h at 20 ± 1 °C in the dark. Sections were then rinsed in PBS, stained with DAPI (DNA-specific fluorescent probe) and then mounted in Mowiol mounting medium (Cold Spring Harb Protoc, 2006).

Immunofluorescence colocalization of B[*a*]P and the lysosomal enzyme cathepsin D: following immunolabelling with the first primary and secondary antibodies (as described above for single labelling), sections were incubated for 1h at RT in PBS containing 2% BSA and 0.5% goat serum (Sforzini et al., 2014). Hence, sections were incubated for 2h at 4°C with the second primary antibody (rabbit polyclonal to cathepsin D (Abcam) 1/100 in PBS containing 1% BSA) and then, after rinsing, in the secondary goat polyclonal to rabbit antibody (DyLight® 594, Abcam, 1/100 in 1% BSA in PBS, 1h, 20±1°C) in the dark. Finally, sections were then rinsed in PBS, stained with DAPI and then mounted.

Immunofluorescent anti-mTOR phospho staining: sections prepared as described above were incubated in a permeabilisation and blocking solution (0.5% Triton X-100, 2% BSA, 0.5% goat serum in PBS, 1 h at 20 ± 1 °C) and then with the primary antibody (anti m-TOR (phospho S2448) antibody, Abcam, 1/100 in PBS containing 1% BSA and 0.05% Triton X-100) overnight at 4 °C in a moist chamber. Sections were then washed three times in PBS (5 min) and the secondary antibody was applied, i.e. polyclonal goat to rabbit (Chromeo) (Abcam) (1/100 in 1% BSA and 0.05% Triton

196 X-100 in PBS) for 1 h at 20 ± 1 °C in the dark. Finally, sections were rinsed in PBS, counterstained
197 with propidium iodide and mounted.
198 Immunofluorescent anti-mTOR staining: sections were incubated in a permeabilisation and
199 blocking solution as described above for the anti-mTOR phospho staining. Then, the primary
200 antibody (anti m-TOR antibody , Abcam, 1/200 in PBS containing 1% BSA and 0.05% Triton X-
201 100) was applied (overnight at 4 °C in a moist chamber). After washing in PBS, sections were
202 incubated with the secondary antibody, i.e. goat polyclonal to rabbit antibody (DyLight® 594)
203 (Abcam) (1/200 in 1% BSA and 0.05% Triton X-100 in PBS) for 1 h at 20 ± 1 °C in the dark.
204 Finally, sections were rinsed in PBS, counterstained with DAPI and mounted.
205 Controls for non-specific staining included sections that were processed in the absence of the
206 primary or secondary antibodies: no positive fluorescent stain was observed. Slides were viewed
207 under 400 × magnification by an inverted photo-microscope (Zeiss Axiovert 100M connected to a
208 digital camera Zeiss AxioCam MRm) equipped for fluorescence microscopy using FITC,
209 Rhodamine and DAPI emission filters. Images were analysed using an image analysis system
210 (Scion Image) that allowed for the quantification of the mean fluorescence intensity. Sections
211 double immunolabelled for B[*a*]P and cathepsin D were viewed under 400 × magnification by Axio
212 Observer and images were taken with ApoTome.2 (Zeiss, Germany).
213
214 *2.5. Sardinia samples and sampling sites: Field study*
215 Mussels (*M. galloprovincialis* Lam.), 4-5 cm in length, were obtained from a farm in Arborea (OR,
216 Sardinia, Italy) and kept in cages (240 mussels per site splitted in five bags) for 28 days (October-
217 November 2013) at three sites along the Sardinian coast: Porto Mannu li Fornelli (40°59'32.1"N
218 8°12'54.5"E -reference site), Cala Reale (41°03'42.7"N 8°17'17.5"E -a small marina), and Porto
219 Torres (40°50'23.1"N 8°24'16.9"E -large industrial and commercial seaport). Mussels were caged in
220 polypropylene mesh bags placed about 4 m under the sea surface. At the end of the period of

221 caging, mussel digestive glands were excised, placed on aluminium cryostat chucks, chilled in
222 super-cooled n-hexane and stored at -80 °C. A large number of biomarkers have been measured in
223 digestive glands of mussels from the three sites; in this study, we investigated in these tissues the
224 response of mTOR.
225
226 *2.6. Univariate statistical analysis*
227 For B[*a*]P experiment, at least five replicates per control and per concentration were analysed. Each
228 replicate consists of the digestive gland from one mussel; the mussels were collected from a
229 separate beaker. For the field study, at least five replicates per caging site were analysed. Each
230 replicate consists of the digestive gland from one mussel; the mussels were collected from five
231 bags. The non-parametric Mann-Whitney *U*-test was used to compare the data from treated mussels
232 with those of the controls ones.
233
234 *2.7. Multivariate statistical analysis*
235 Biomarker data for mussels exposed to B[*a*]P were analysed using non-parametric multivariate
236 analysis software, PRIMER v 6 (PRIMER-E Ltd., Plymouth, UK; Clarke, 1999; Clarke &
237 Warwick, 2001). All data were log transformed [$\log_n(1+x)$] and standardised to the same scale.
238 Principal component analysis (PCA) and hierarchical cluster analysis, derived from Euclidean
239 distance similarity matrices were used to visualise dissimilarities between sample groups. The
240 results were further tested for significance using analysis of similarity (PRIMER v6 - ANOSIM),
241 which is an approximate analogue of the univariate ANOVA and reflects on differences between
242 treatment groups in contrast to differences among replicates within samples (the *R* statistic). Under
243 the null hypothesis H_0 (“no difference between samples”), $R = 0$ and this was tested by a non-
244 parametric permutations approach; there should be little or no effect on the average R value if the
245 labels identifying which replicates belong to which samples are randomly rearranged.

Finally, in order to map integrated biomarker data onto "health status space" (measured as system complexity - connectance Cv%) first principal components (PC1) for the biomarker data were derived using PRIMER v6 and then plotted against the complexity values (as a measure of cellular well-being) for each treatment (Allen and Moore, 2004; Moore et al., 2006a; Sforzini et al., 2015, 2017).

2.8. Network modelling of biomarker data

2.8.1. Model description

The generic cell model described by Moore (2010) has been developed from extensive published data in the environmental toxicology and biomedical literature, and the large-scale organisation of metabolic networks (Cuervo, 2004; Di Giulio & Hinton, 2008; Jeong et al., 2000; Klionsky & Emr, 2000). The generic cellular interaction network was constructed around the essential processes of feeding, excretion and energy metabolism. Protein synthesis and degradation, including lysosomal autophagy, are also incorporated in the model as are the major protective systems (Cuervo, 2004; Di Giulio & Hinton, 2008; Livingstone et al., 2000; Moore, 2008; Moore et al., 2015). A modified subset of the generic model was used in this investigation in order to accommodate the available data (Fig. 8). The directed cellular physiological networks were constructed using Cytoscape 3.3.0 (Shannon et al., 2003).

2.8.2. Analysis of cell system complexity

Whole system complexity in the directed cellular physiological network was evaluated using connectedness (Bonchev, 2003). Topological complexity was measured as connectedness or connectance (C_V %) is the ratio between the number of links E in the interaction network and the number of links in the complete graph having the same number of nodes or vertices (*V*) (Bonchev, 2003). Connectedness relates the number of nodes (vertices) *V* and links or edges (arcs in a directed

link) E where the connectance ratio, C_V, of a directed graph (digraph) with V nodes or vertices is then:

$C_V = [(1 / max\ (CV)]||E||\ x\ 100$

which reduces to: $CV = (||E|| / V^2)\ x\ 100$

for typical digraphs that allow every node to connect to every other node, where $||E||$ is the nearest integer function of E (Davis, 1997). This method uses the sum of the edge weights rather than the edge count and allows for self-loops or arcs as with the autophagy process (Fig. 8).

Transformed biomarker data were used to attribute proportional weight values to the interactions (edges) between cellular physiological processes (nodes) as shown in Table 1; and to the nodes, as node size (Fig. 8). The various biomarker mean values were standardised to a proportion of Control values. These standardised biomarker values (x) were used for biomarkers that normally decrease with pathology (e.g., lysosomal membrane stability & mTORC1), while biomarkers that normally increase with pathology (e.g., neutral lipid, lysosomal/cytoplasmic volume ratio & lipofuscin) were further transformed to (x^{-1}). These values were normalised using $\log_{10}$ transformation and then inputted as the weight values for the network interactions (edges/links). The standardised biomarker values were used to set node size for comparisons of network topology (see Fig. 8). The Kruskall-Wallis test were applied to the proportional edge (interaction) values of the treatment groups.

3. Results

3.1. Cytochemical and immunohistochemical analysis

The concentrations of B[*a*]P utilised in this study, after 3 d of exposure, did not provoke any effect on vitality of mussels (data not shown).

Immunofluorescence labelling of digestive glands of B[*a*]P exposed mussel with the anti-PAHs antibody was positive (Fig. 1B-D); no immunopositivity was detected in control animals (Fig. 1A). Double immunolabelling of sections with antibodies against PAHs and cathepsin D demonstrated

296 that B[*a*]P accumulated inside lysosomes (Fig. 1F). Quantification of the B[*a*]P fluorescence signal
297 by digital imaging (Fig. 1E) showed a significant increase in fluorescence intensity in animals
298 exposed to all the experimental conditions, with respect to controls; however, the most intense
299 staining was found at the lower B[*a*]P concentration (5 μg/L). The examination of unstained serial
300 sections of B[*a*]P exposed mussels under UV light highlighted the presence of numerous white-blue
301 fluorescent droplets; the fluorescence was minimal in the digestive glands of mussels exposed to 5
302 μg/L and increased from 50 μg/L to 100 μg/L B[*a*]P (Fig. 2).
303 B[*a*]P accumulated in the digestive glands of exposed mussels provoked significant alterations to
304 the lysosomal vacuolar system (Fig. 3). As shown in Fig. 3A, a decrease of LMS was observed at
305 all the concentrations, that was significant at 50 μg/L and 100 μg/L B[*a*]P. At the higher B[*a*]P
306 concentrations i.e. 50 μg/L and 100 μg/L B[*a*]P, a significant increase of the lysosomal/cytoplasmic
307 volume ratio, a biomarker of tissue damage, was also observed (+44% and +42% respectively, with
308 respect to controls) (Fig. 3B).
309 The use of an anti-mTOR antibody phosphorylated on S2448 revealed in digestive gland sections of
310 control mussels an immunopositive reaction; in particular, the fluorescence signal was mainly
311 located in the perinuclear region of the tubule epithelial cells (Fig. 4A). The immunohistochemical
312 data demonstrated that in the digestive gland cells of mussels exposed to all the different B[*a*]P
313 concentrations, the level of phosphorylated mTOR significantly decreased (Fig. 4F); stronger
314 effects were observed at 50 μg/L B[*a*]P and in particular at 100 μg/L B[*a*]P (Fig. 4C-E, F). The
315 specificity of this mTOR antibody within the mussel digestive gland was demonstrated by western
316 blot analysis; these results also confirm the dephosphorylation of the protein in B[*a*]P exposed
317 mussels (see Supplementary Information for the details of the method and western blot figure -Fig.
318 S1).

The results reported in Fig. 5 clearly demonstrate that mTOR protein level showed a strong increase in the cytoplasm of the animals exposed to B[a]P, reaching the highest values in the digestive gland of mussels treated with B[a]P 50-100 µg/L.

When the immunofluorescence staining with the anti-mTOR phosphorylated antibody was performed in digestive gland sections of mussels caged along the Sardinian coast, the analysis revealed a strong inactivation of mTOR in Porto Torres (a polluted areas) with respect to the reference site (Porto Mannu li Fornelli) (Fig. 6A, C).

3.2. Multivariate analysis of biomarker reactions

Principal component (PCA) and hierarchical cluster analysis of all the biomarker reactions showed that B[*a*]P had a detrimental effect on the digestive cells of mussels (Fig. 7). Analysis of similarity shows that these clusters were significantly different (ANOSIM, R Statistic: $R = 0.856$, $P = 0.001$). Treatments were clearly separated ($P < 0.01$) with the exceptions of the 50 and 100 µg/L, which overlapped but were still significantly different ($P < 0.05$). Multiple regression analysis of the biomarker data indicated that all of the biological parameters were significantly correlated ($P < 0.01$).

3.3. Network modelling biomarker reactions to B[a]P treatment

Inputting the biomarker data into the directed cellular interaction network (digraph) model (Fig. 8) allowed the determination of the system complexity. Complexity values as connectance ratio (Cv%) for the experimental treatments are shown in Fig. 8, with a considerable significant loss in connectivity in the B[a]P treated conditions compared with the controls ($P = 5.52 \times 10^{-8}$, Kruskal-Wallis test).

The control and treated network topologies differ in node size and are significantly different as demonstrated by the ANOSIM and PCA/cluster analysis (Fig. 7). The determination of node degree

indicated that autophagy was the most highly connected node with 8 degrees (i.e., summation of 3 out-arc, 4 in-arcs and 1 loop), making it an important physiological hub (Fig. 8). System complexity (connectance %) was strongly correlated with the concentration of B[a]P (inverse), lysosomal stability (direct), first principal component (direct) and DNA damage (inverse; COMET assay data from Banni et al, 2017; see also Canova et al, 1998) as shown in Fig. 9.

4. Discussion

In this study, we investigated the reactions of the lysosomal vacuolar system and the possible involvement of mTOR in their regulation in the digestive gland of mussels *M. galloprovincialis*. exposed to B[*a*]P. The digestive gland of bivalve mollusks is the principal site of digestion and absorption (Bayne, 2009); and represents the major tissue involved in the accumulation and detoxification of organic and inorganic environmental contaminants (Banni et al., 2016; Gomes et al., 2012; Moore, et al., 2007; Viarengo et al., 1981). The lysosomal vacuolar system of the digestive gland cells is well-developed, providing for most of the above mentioned functions (Dimitriadis et al., 2004; Moore, 1988).

B[*a*]P accumulated in digestive tubule epithelial cells of exposed mussels, as revealed by immunohistochemical analysis of digestive gland tissue sections by using an anti-PAHs antibody. This method, recently developed in earthworm tissues (Sforzini et al., 2014), proved to be a reliable tool for demonstrating the presence and the cellular distribution of B[*a*]P in animals exposed to soils contaminated by even a minimal amount of this chemical (0.1 ppm). In particular, the use of the double immunohistochemical method for co-localization of B[*a*]P and the cathepsin D (a lysosomal protease highly conserved throughout lower and higher eukaryotes - Phillips et al., 2006) demonstrated the lysosomal accumulation of the organic xenobiotic compound.

Interestingly, the fluorescence intensity was more intense in the digestive glands from mussels exposed to the lowest B[*a*]P concentration (5 µg/L). Previous studies demonstrated that different

PAHs such as B[*a*]P and fluoranthene, when present in the tissues at high concentrations, are progressively compartmentalised in lipid rich vesicles, with fluorescence properties (fluorescence intensity directly related to the chemical amount) (Allison and Mallucci, 1964; Moore et al., 2007; Plant et al., 1985; Sforzini et al., 2014). These chemicals are highly lipophilic and are known to induce an alteration of fatty acid metabolism (lipidosis) (De Coster and van Larebeke, 2012; Moore et al., 2007); lipids are then internalised into the lysosomes by autophagic uptake (Moore, 1988; Podechard et al., 2009). In mussels exposed to all the different concentrations of B[*a*]P, a significant increase was observed in lysosomal neutral lipid content of the digestive gland cells (Fig. S2 - see Supplementary Information). The comparison between serial sections of tissues from mussels exposed to B[*a*]P 50, 100 µg/L stained with Oil-Red O (lipid soluble dye commonly used for the histochemical staining of neutral lipids in cryostat tissue sections -Bayliss High, 1984; Moore, 1988) in bright-field and unstained sections by UV-fluorescence, highlighted that the distribution of the B[*a*]P fluorescent droplets in the digestive gland cells corresponds to that of the neutral lipid containing vesicles (Fig. 10). Recent studies have reported difficulty in labelling target molecules in lipid droplets by immunofluorescence methods, probably because of the reduced accessibility of these compartments to the antibodies (DiDonato and Brasaemle, 2003; Ohsaki et al., 2005; Sforzini et al., 2014). Chemical results support this hypothesis, showing that the amount of B[*a*]P accumulated in the digestive gland of exposed mussels increased with increasing dose; in addition, the lipid concentration also increased with increasing exposure concentrations (Banni et al., 2017).

Lysosomes of B[*a*]P exposed mussels showed relevant perturbations in their activity. LMS was reduced in animals exposed to 5 µg/L B[*a*]P but stronger effects were observed at 50 and 100 µg/L. Lysosomes are the target for many pollutants (both organic xenobiotics as well toxic metals); the chemicals accumulated in lysosomes may perturb normal function and damage the lysosomal membrane (Moore et al., 2006b; Sforzini et al., 2014; Viarengo et al., 1981). Pathological reactions

involving the lysosomal system are also often linked to augmented autophagic sequestration of cytoplasmic components (e.g. autophagic accumulation of neutral lipids) and the removal of damaged organelles and proteins (which are degraded in lysosomes) (Glick, et al., 2010; Moore, 2008). In vertebrates, quinone derivates, produced during B[*a*]P metabolic processes, generate reactive oxygen species (ROS) by redox cycling, which oxidatively altered DNA, protein, and antioxidant enzymes (Kim and Lee, 1997). B[a]P is metabolized predominantly to quinones by mussel digestive gland microsomes (Livingstone et al., 1988; Stegeman, 1985). Although the hydrocarbon metabolism in molluscs is slow and the rate-limiting cytochrome P450 may be responsible for this (Livingstone, 1998), previous studies have demonstrated changes in antioxidant enzymes and peroxisomal proliferation with exposure of mussels to B[*a*]P (Livingstone et al., 1990; Orbea et al., 2002), indicating an enhancement of oxyradical generation. In mussels exposed to all the different concentration of B[*a*]P utilised in this study, Banni et al. (2017) demonstrated an increase of lipofuscin accumulated in lysosomes of digestive gland cells. It is likely that reactive free radicals contribute to the damaging effects on the lysosomal membrane and build-up of lipofuscin (end product of oxidative attack on lipids and proteins) (Viarengo, 1989; Moore, 2008; Winston et al., 1996).

In this context, the autophagy may have a protective role in the context of (oxidative) stress through the degradation and recycling of oxidised proteins and damaged organelles (Cuervo, 2004). However, an excessive autophagic rate has been shown to have deleterious consequences for tissue/organism health (Levine and Kroemer, 2008). At the higher B[*a*]P concentrations, a significant enhancement of L/C volume ratio was also observed. These data indicate that the animals are catabolic i.e. the autophagic process is highly stimulated and the catabolism of the macromolecules is not compensated by protein synthesis. The (oxidative) damage to cellular components may have contributed to decrease protein synthesis (Viarengo, 1989; Winston et al.,

418 1996; Moore et al., 2006a). The reduction of the cytoplasm of the cells may lead a loss of their
419 proper functionality with negative consequences on digestive gland physiology.
420 Overall, these results confirm that digestive cell lysosomes are the targets for toxic chemicals and
421 they are also sites of their accumulation. B[*a*]P stimulated the lysosomal fatty acid accumulation
422 and at the higher concentrations was stored in these compartments. Moreover, at the higher doses,
423 B[*a*]P also overstimulates the autophagic process leading to cell catabolism and thus tissue
424 pathology. One of the possible processes that could explain the observed effects is the mTOR signal
425 transduction pathway. mTOR (mechanistic target of rapamycin) is an evolutionarily-conserved
426 serine/threonine protein kinase that represents the central node of a highly conserved signalling
427 network regulating cell growth in response to nutrients, hormones and stresses (Jung et al., 2010).
428 mTOR is found in two functionally distinct complexes, mTORC1 and mTORC2. In particular, the
429 phosphorylated active form of TORC1 mediates temporal control of cell growth by activating
430 anabolic processes such as transcription, ribosome biogenesis, protein synthesis; and by inhibiting
431 catabolic processes such as autophagy (Dowling et al., 2010; Soulard et al., 2009). In mammals a
432 lot of studies have been devoted to investigate mTOR regulators. The dysregulation of mTOR
433 signalling is implicated in a number of human diseases including cancer (Dowling et al., 2010). In
434 invertebrates, the research on TOR signalling, particularly in contaminant exposed organisms is an
435 area where much remains to be explored (Soulard et al., 2009).
436 Recently, Copp et al. (2009) showed that mTOR is phosphorylated differentially when associated
437 with mTORC1 and mTORC2; specifically, they found that mTORC1 contains mTOR
438 phosphorylated predominantly on S2448. The immunofluorescence labelling of control digestive
439 gland sections using an anti-mTOR antibody phosphorylated on S2448 revealed an immunopositive
440 reaction; in particular, the fluorescence signal was mainly located in the perinuclear region of the
441 tubule epithelial cells. These results are in line with other studies showing that mTORC1 in
442 different kind of cells (such as trypanosomes, yeast and mammalian cells) localizes mainly to the

443 nucleus (Barquilla et al., 2008; Li et al., 2006). When the digestive gland cells of mussels exposed
444 to all the different B[*a*]P concentrations were reacted for the anti-mTOR (phospho S2448) antibody,
445 the fluorescent signal decreased; at 50 µg/L B[*a*]P and in particular at 100 µg/L B[*a*]P, i.e.
446 concentrations that provoked a sustained increase of the cellular catabolic rate, we observed
447 dramatic changes. Although the mechanisms that regulate the mTOR dephosphorylation are not till
448 now fully understood, the possibility that B[*a*]P stimulating ROS production may affect mTOR
449 activities is in line with recently reported results (Chen et al., 2010; Moore, 2008). It is important to
450 mention that the total amount of mTOR showed a significant increase in mussels exposed to the
451 different B[a]P concentrations (Fig. 5). This fact emphasises the importance of mTOR
452 phosphorylation/dephosphorylation in the regulation of cell metabolism.
453 An important aspect of this study was to investigate if the data obtained could have a general value,
454 i.e. if the level of phosphorylation of mTOR (activation/inhibition) could be also observed in
455 mussels exposed to field environmental conditions. To this end, we analysed mussels that were
456 caged for 28d in different sites along the Sardinian coast characterized by different levels of
457 contamination i.e. Fornelli, the reference site, Cala Reale, a small marina, and Porto Torres, large
458 industrial and commercial seaport contaminated by PAHs and heavy metals. An intense mTORC1
459 fluorescent signal was observed in the perinuclear area of the digestive gland cells of mussels caged
460 in the reference site (Fornelli); immunofluorescence staining showed a decrease in mussels caged in
461 Cala Reale. In mussels caged in Porto Torres, the level of mTOR phosphorylation was extremely
462 low; in the digestive glands of the same animals we have found a strong decrease of LMS and an
463 enhancement of L/C volume ratio; as well oxidative stress damage (Banni et al., manuscript in
464 preparation). The “picture” depicted by the field experiment is very similar to that observed in the
465 lab one.
466 Principal Component Analysis (PCA) is an effective method for integrating biomarker data into a
467 “health status space” reducing the multi-dimensionality of the problem to a simple two dimensional

representation (Chatfield and Collins, 1980; Allen and Moore, 2004). PCA is commonly used as a cluster analysis tool and effectively captures the variability in a dataset in terms of principal components, and previously PCA has facilitated modelling the integrated responses of multiple biomarkers in the context of "health status space" (Allen and Moore, 2004; Moore et al., 2006a). These models have shown that there is a strong relationship between LMS, as an indicator of cellular health, and other combined biomarker responses (Allen & Moore, 2004; Moore et al., 2006a; Sforzini et al., 2015, 2017).

However, PCA and cluster analysis does not integrate the various biomarkers in a functionally meaningful way, and is only the first stage in developing numerical and network models for environmental impact on the health of sentinel animals such as mussels and earthworms (Allen and Moore, 2004; Moore, 2010; Sforzini et al., 2015, 2017). In order to encapsulate the cellular physiological processes, it is necessary to interconnect the biomarker data into a logical framework. This was done using a network model of the physiological/pathological processes known to occur in the digestive cells. Complexity is a measure of the interconnectedness of the network and can be used as an indicator of homeostasis (Lewis et al., 1992; Moore, 2010; Moore et al., 2015; Sedivy, 1999). Complexity of the whole system increases when sub-systems, such as detoxication and anti-oxidant protective processes, augmented autophagy, protein degradation and induction of stress proteins, are up-regulated and start to interact significantly as part of a response to low-level stress (i.e., biphasic or hormetic response; Moore, 2010; Moore et al., 2015). However, with increasing severity of stress, cell injury and higher-level functional impairment lead to physiological dysfunction, pathology and breakdown of the whole interaction network with consequent loss of complexity (Moore, 2010). Consequently, inputting the biomarker data from the B[a]P exposure experiment into a directed cell physiology network model showed that there was a statistically significant reduction in system complexity with increasing tissue B[a]P, indicating decreased homeostasis and health status (Fig. 9; Table 1). Network topology was also significantly different in

493 terms of node size (Fig. 8). The model demonstrates that autophagy is an important highly
494 connected hub in the cellular physiology of the system being tested, which lends support to the
495 overall hypothesis, namely, that autophagy, lysosomal function and mTOR signaling are
496 intrinsically interlinked in responses/reactions to stress (Fig. 8). The strong correlations between
497 network complexity, B[*a*]P concentration, lysosomal stability and first principal component further
498 support the use of system complexity as a measure of cellular homeostasis (Fig. 9).
499 The network approach supports the hypothesis that stress leading to pathology results in a loss of
500 system complexity as previously described by Moore (2010). Consequently, cellular networks can
501 be used to integrate information from biomarker data; and to direct the selection of biomarkers and
502 design of experiments, in order to develop suites of tests that will demonstrate which links are
503 active or inactive, and to what degree. This provides mathematical formalism for an objective
504 evaluation of health status for potential use in risk assessment (Moore, 2002, Moore et al., 2004b).
505 Cellular interaction networks also have considerable potential for integrating multi-biomarker data
506 for evaluation of whole system "health status" (Moore, 2010). The strong correlation between
507 system complexity and DNA damage indicates that this type of modelling has potential for
508 predicting cellular pathological endpoints (Canova et al., 1998; Fig. 9).
509 Finally, the network model facilitates the development of a mechanistic framework that
510 encapsulates the interrelated patho-physiological processes that are involved in the cellular
511 reactions to the B[*a*]P. These processes are described diagrammatically in Figure 11, although all of
512 them are evolutionarily highly conserved, some are not yet confirmed to occur in molluscs (i.e.,
513 mTOR links with endocytosis and MDR/Pgp40 multi-drug resistance transporter). This diagram
514 shows the linkages between endocytotic uptake of B[*a*]P with natural particles, transfer to the
515 lysosomal system, where accumulation will be further facilitated by P-glycoprotein (MDR-Pgp40)
516 in the lysosomal membrane (Minier & Moore, 1996a, b; Yang et al., 2002). Accumulation of B[*a*]P
517 and lipid in the lysosomal compartment results in ROS generation and formation of lipofuscin

518 (stress or age pigment) (Brunk & Terman, 2002; Moore et al., 2006a). Oxidative stress may have a
519 positive feedback inhibiting mTORC1 and enhancing authophagy (Brunk & Terman, 2002; Chen et
520 al., 2010; Moore et al., 2006a, 2015). Inhibition of mTORC1 will also inhibit endocytosis,
521 lysosomal membrane stability and activate Pgp40 (Boya, 2012; Flinn & Backer, 2010; Jiang & Liu,
522 2008). The increased flux of ROS will also contribute to oxidative damage to DNA (Canova et al.,
523 1998); and enhanced autophagy may engulf portions of damaged and undamaged genomic material
524 through partial nuclear autophagy (Buckland-Nicks & Hodgson, 2005; Mochida et al., 2015).
525 Autophagy of nuclear DNA may contribute to autophagic and/or apoptotic cell death as a
526 pathological endpoint (Lowe, 1988); and may be protective against the development of digestive
527 gland tumours, which are extremely rare in molluscs (Khudoleĭ & Sirenko, 1977).
528

529 ## 5. Conclusions

530 Overall, the data obtained in this work demonstrate that the signal transduction pathways linked to
531 mTOR (and in particular to mTORC1) could play an important role to determine the set of the
532 pathological effects that render the organisms "catabolic" and therefore no more able to sustain a
533 correct scope for growth. The probable role of mTOR in cell signalling and the regulation of the
534 cellular responses to the contaminants has been confirmed in a field study, where in the digestive
535 gland of mussels sampled from contaminated sites there was an inactivation of mTOR. Obviously,
536 as mentioned above, part of the shown effects (and others such as DNA damage) may depend on the
537 direct effect of the toxic chemical on the different cellular components. The analysis of the data by
538 the network connectedness demonstrates that autophagy, lysosomal function and mTOR signalling
539 are intrinsically interlinked in responses/reactions to stress. This network approach supports the
540 hypothesis that stress leading to pathology results in a loss of system complexity (Moore, 2010).
541 Cellular interaction networks also have considerable potential for integrating multi-biomarker data

for evaluation of whole system "health status" and for potential use in risk assessment (Moore, 2010).

Acknowledgements

This study was supported financially by Natural Environment Research Council (NERC), UK (Grant No.NE/L006782/1; PI: ANJ).

References

Abele, D., Brey, T., Philipp, E., 2009. Bivalve models of aging and the determination of molluscan lifespans. Exp. Gerontol. 44, 307-315.

Allen, J.I., McVeigh, A., 2004. Towards computational models of cells for environmental toxicology. J. Mol. Histol. 35,697-706.

Allen, J.I., Moore, M.N., 2004. Environmental prognostics: is the current use of biomarkers appropriate for environmental risk evaluation. Mar. Environ. Res. 58, 227-232.

Allison, A.C., Mallucci, L., 1964. Uptake of hydrocarbon carcinogens by lysosomes. Nature 203, 1024-1027.

Appelqvist, H., Wäster, P., Kågedal, K., Öllinger, K., 2013. The lysosome: from waste bag to potential therapeutic target. J. Mol. Cell. Biol. 5, 214-226.

Banni, M., Sforzini, S., Balbi, T., Corsi, I., Viarengo, A., Canesi, L., 2016. Combined effects of n-TiO_2 and 2,3,7,8-TCDD in *Mytilus galloprovincialis* digestive gland: A transcriptomic and immunohistochemical study. Environ Res. 145, 135-144.

Banni, M., Sforzini, S., Arlt, V. M., Barranger, A., Dallas, L. J., Oliveri, C., Aminot, Y., Pacchioni, B., Millino, C., Lanfranchi, G., Readman, J. W., Moore, M. N., Viarengo, A., Jha, A. N., 2017. Assessing the impact of Benzo[a]pyrene on Marine Mussels: Application of a novel

566 targeted low density microarray complementing classical biomarker responses. PLoS ONE
567 12(6), e0178460. https://doi.org/10.1371/journal.pone.0178460.
568 Barquilla, A., Crespo, J.L., Navarro, M:, 2008. Rapamycin inhibits trypanosome cell growth by
569 preventing TOR complex 2 formation. Proc. Natl. Acad. Sci. U S A 105,14579-14584.
570 Bayliss High, O., 1984. Lipid Histochemistry (Royal Microscopical Society, Microscopy
571 Handbooks, No. 6). Oxford University Press, Oxford.
572 Bayne, B.L., Moore, M.N. and Koehn, R.K., 1980. Lysosomes and the response by *Mytilus edulis*
573 to an increase in salinity. Mar. Biol. Letters 2, 193-204.
574 Bayne, B.L., 2009. Marine Mussels: Their Ecology and Physiology, Cambridge University Press,
575 528 p.
576 Bignell, J.P., Stentiford, G.D., Taylor, N. G., Lyons, B.P., 2011. Histopathology of mussels
577 (*Mytilus* sp.) from the Tamar Estuary, UK. Mar. Environ. Res. 72, 25-32.
578 Bonchev, D., 2003. Complexity of protein-protein interaction networks, complexes, and pathways.
579 In: Handbook of proteomic methods (Ed PM Conn) pp 451-462. Humana Press, Totowa, New
580 Jersey.
581 Boya, P., 2012. Lysosomal function and dysfunction: mechanism and disease. Antiox. Redox
582 Signaling 17, 766-774.
583 Brunk, U.T., Terman, A., 2002. Lipofuscin: mechanisms of age-related accumulation and influence
584 on cell function. Free Rad. Biol. Med. 33, 11-619.
585 Buckland-Nicks, J., Hodgson, A.N., 2005. Paraspermatogenesis of cerithioidean snails: retention of
586 an acrosome and nuclear remnant. J. Morphology 264, 314-326.
587 Canova, S., Degan, P., Peters, L.D., Livingstone, D.R., Voltan, R., Venier, P., 1998. Tissue dose,
588 DNA adducts, oxidative DNA damage and CYP1A-immunopositive proteins in mussels
589 exposed to waterborne benzo[a]pyrene. Mutation Res/Fundamental and Molecular
590 Mechanisms of Mutagenesis 399, 17-30.

591 Chatfield, C., Collins, A.J., 1980. Introduction to Multivariate Analysis. Chapman and Hall,
592 London.
593 Chen, L., Xu, B., Liu, L., Luo, Y., Yin, J., Zhou, H., Chen, W., Shen, T., Han, X., Huang, S., 2010.
594 Hydrogen peroxide inhibits mTOR signaling by activation of AMPKa leading to apoptosis of
595 neuronal cells. Lab. Invest. 90, 762-773.
596 Clarke, K.R., 1999. Non-metric multivariate analysis in community-level ecotoxicology. Environ.
597 Toxicol. Chem. 18, 117-127.
598 Clarke, K.R., Warwick, R.M., 2001. Change in marine communities: an approach to statistical
599 analysis and interpretation. PRIMER-є, Plymouth, UK.
600 Cold Spring Harb Protoc, 2006. doi: 10.1101/pdb.rec10255.
601 Copp, J., Manning, G., Hunter, T., 2009. TORC-specific phosphorylation of mammalian target of
602 rapamycin (mTOR): phospho-Ser2481 is a marker for intact mTOR signaling complex 2.
603 Cancer Res. 69, 1821-1827.
604 Cuervo, A.M., 2004. Autophagy: in sickness and in health. TRENDS Cell Biol. 14, 70-77.
605 Davis, M.W., 1997. Complexity formalisms, order and disorder in the structure of art. In:
606 Evolutionary Programming VI, Lecture Notes in Computer Science (Editors: Angeline PJ,
607 Reynolds, McDonnell JR, Eberhart R), Vol. 1213, Springer International Publishing AG,
608 Switzerland. pp 1-12.
609 De Coster, S., van Larebeke, N., 2012. Endocrine-disrupting chemicals: associated disorders and
610 mechanisms of action. J. Environ. Public Health 2012:713696.
611 Di Giulio, R.T., Hinton, D.E., Editors, 2008. The toxicology of fishes. Taylor and Francis, London,
612 New York, Singapore, Melbourne, 1071 p.
613 DiDonato, D., Brasaemle, D.L., 2003. Fixation methods for the study of lipid droplets by
614 immunofluorescence microscopy. J. Histochem. Cytochem. 51, 773-780.

615 Dimitriadis, V.K., Domouhtsidou, G.P., Cajaraville, M.P., 2004. Cytochemical and histochemical
616 aspects of the digestive gland cells of the mussel *Mytilus galloprovincialis* (L.) in relation to
617 function. J. Mol. Histol. 35, 501-509.
618 Dowling, R.J., Topisirovic, I., Fonseca, B.D., Sonenberg, N., 2010. Dissecting the role of mTOR:
619 lessons from mTOR inhibitors. Biochim. Biophys. Acta 1804, 433-439.
620 Fernández, F.P., Labrador, V., Pérez Martín, J.M., Hazen, M.J., 2005. Cytotoxic effects in
621 mammalian Vero cells exposed to pentachlorophenol. Toxicology 210, 37-44.
622 Flinn, R.J., Backer, J.M., 2010. mTORC1 signals from late endosomes: taking a TOR of the
623 endocytic system. Cell Cycle, 9, 1869-1870.
624 Glick, D., Barth, S., Macleod, K. F., 2010. Autophagy: cellular and molecular mechanisms. J.
625 Pathol. 221, 3-12.
626 Gliński, Z., Jarosz, J., 1997. Molluscan immune defenses. Arch. Immunol. Ther. Exp. (Warsz). 45,
627 149-155.
628 Gomes, T., Pereira, C.G., Cardoso, C., Pinheiro, J.P., Cancio, I., Bebianno, M.J., 2012.
629 Accumulation and toxicity of copper oxide nanoparticles in the digestive gland of *Mytilus*
630 *galloprovincialis*. Aquat Toxicol. 118-119, 72-79.
631 Jeong, H., Tombor, B., Albert, R., Oltval, Z.N., Barábasi, A.-L., 2000. The large scale organization
632 of metabolic networks. Nature 407, 651-654.
633 Jiang, B.H., Liu, L.Z., 2008. Role of mTOR in anticancer drug resistance: perspectives for
634 improved drug treatment. Drug Resist. Updates 11, 63-76.
635 Jung, C.H., Ro, S.H., Cao, J., Otto, N.M., Kim, D.H., 2010. mTOR regulation of autophagy. FEBS
636 Lett. 584, 1287-1295.
637 Khudoleĭ, V.V., Sirenko, O.A., 1977. Development of tumors in *Unio pictorum* bivalve mollusks
638 under the influence of N-nitroso compounds. Biulleten'eksperimental'noi biologii i meditsiny
639 83, 577-579.

640 Kim, K.B., Lee, B.M., 1997. Oxidative stress to DNA, protein, and antioxidant enzymes
641 (superoxide dismutase and catalase) in rats treated with benzo(a)pyrene. Cancer Lett. 113,
642 205-212.
643 Klionsky, D.J., Emr, S.D., 2000. Autophagy as a regulated pathway of cellular degradation. Science
644 290, 1717-1721.
645 Laplante, M., Sabatini, D. M., 2012. mTOR signaling in growth control and disease. Cell. 149, 274-
646 293.
647 Levine, B., Kroemer, G., 2008. Autophagy in the Pathogenesis of Disease. Cell. 132, 27-42.
648 Lewis, A., Lipsitz, M.D., Ary, L., Goldberger, M.D., 1992. Loss of "complexity" and aging:
649 potential applications of fractals and chaos theory to senescence. J. Amer. Med. Assoc. 267,
650 1806-1809.
651 Li, H., Tsang, C.K., Watkins, M., Bertram, P.G., Zheng, X.F., 2006. Nutrient regulates Tor1 nuclear
652 localization and association with rDNA promoter. Nature 442, 1058-1061.
653 Livingstone, D.R., 1998. The fate of organic xenobiotics in aquatic ecosystems: quantitative and
654 qualitative differences in biotransformation by invertebrates and fish. Comp. Biochem.
655 Physiol. A Mol. Integr. Physiol. 120, 43-49.
656 Livingstone, D.R., Garcia Martinez, P., Stegeman, J.J, Winston, G.W., 1988. Benzo[a]pyrene
657 metabolism and aspects of oxygen radical generation in the common mussel, *Mytilus edulis*.
658 Biochem. Soc. Trans. 16, 779.
659 Livingstone, D.R., Garcia Martinez, P., Michel, X., Narbonne, J. F., O'Hara, S., Ribera, D.,
660 Winston, G.W., 1990. Oxyradical Production as a Pollution-Mediated Mechanism of Toxicity
661 in the Common Mussel, *Mytilus edulis* L., and Other Molluscs. Functional Ecology Vol. 4,
662 No. 3, New Horizons in Ecotoxicology, pp. 415-424.
663 Livingstone, D.R., Chipman, J.K., Lowe, D.M., Minier, C., Mitchelmore, C.L., Moore, M.N.,
664 Peters, L.D., Pipe, R.K., 2000. Development of biomarkers to detect the effects of organic

665 pollution on aquatic invertebrates: recent molecular, genotoxic, cellular and immunological
666 studies on the common mussel (*Mytilus edulis* L.) and other mytilids. Int. J. Environ. Pollut.
667 13, 56-91.
668 Lowe, D.M., 1988. Alterations in cellular structure of *Mytilus edulis* resulting from exposure to
669 environmental contaminants under field and experimental conditions. Mar. Ecol. Prog. Ser.
670 46, 91-100.
671 Manodori, L., Gambaro, A., Piazza, R., Ferrari, S., Stortini, A.M., Moret, I., Capodaglio, G., 2006.
672 PCBs and PAHs in sea-surface microlayer and sub-surface water samples of the Venice
673 Lagoon (Italy). Mar. Pollut. Bull. 52, 184-192.
674 Minier, C., Moore, M.N., 1996a. Multixenobiotic resistance in mussel blood cells. Mar. Environ.
675 Res. 42, 389-392.
676 Minier, C., Moore, M.N., 1996b. Rhodamine B accumulation and MXR protein expression in
677 mussel blood cells: effects of exposure to vincristine. Mar. Ecol. Prog. Ser. 142, 165-173.
678 Mochida, K., Oikawa, Y., Kimura, Y., Kirisako, H., Hirano, H., Ohsumi, Y., Nakatogawa, H.,
679 2015. Receptor-mediated selective autophagy degrades the endoplasmic reticulum and the
680 nucleus. Nature 522, 59-362.
681 Moore, M.N., 1976. Cytochemical demonstration of latency of lysosomal hydrolases in digestive
682 gland cells of the common mussel *Mytilus edulis*, and changes induced by thermal stress. Cell
683 Tissue Res. 175, 279-287.
684 Moore, M.N., 1988. Cytochemical responses of the lysosomal system and NADPH-
685 ferrihemoprotein reductase in molluscan digestive cells to environmental and experimental
686 exposure to xenobiotics. Mar. Ecol. Prog. Ser. 46, 81-89.
687 Moore, M.N., 2002. Biocomplexity: the post-genome challenge in ecotoxicology. Aquat. Toxicol.
688 59, 1-15.

689 Moore, M.N., 2004. Diet restriction induced autophagy: a novel protective system against
690 oxidative- and pollutant-stress and cell injury. Mar. Environ. Res. 58, 603-607.
691 Moore, M.N., 2008. Autophagy as a second level protective process in conferring resistance to
692 environmentally-induced oxidative stress. Autophagy 4, 254-256.
693 Moore, M.N., 2010. Is toxicological pathology characterised by a loss of system complexity? Mar.
694 Environ. Res. 69, S37-S41.
695 Moore, M.N., Clarke, K.R., 1982. Use of microstereology and cytochemical staining to determine
696 the effects of crude oil-derived aromatic hydrocarbons on lysosomal structure and function in
697 a marine bivalve mollusc *Mytilus edulis*. Histochem. J. 14, 713-718.
698 Moore, M.N., Noble, D., 2004. Computational modelling of cell & tissue processes and function. J.
699 Mol. Histol. 35, 655-658.
700 Moore, M.N., Koehn R.K. and Bayne, B.L., 1980. Leucine aminopeptidase (aminopeptidase-1), N-
701 acetyl-β-hexosaminidase and lysosomes in the mussel *Mytilus edulis* L., in response to salinity
702 changes. J. Exp. Zool. 214, 239-249.
703 Moore, M.N., Soverchia, C. and Thomas, M., 1996. Enhanced lysosomal autophagy of intracellular
704 proteins by xenobiotics in living molluscan blood cells. In: Proc. 10 th International Congress
705 Histochem. Cytochem., Acta Histchem. Cytochem., 29 (Supplement), 947-948.
706 Moore, M.N, Lowe, D.M., Kohler, A., 2004a. Biological effects of contaminants: Measurements of
707 lysosomal membrane stability. ICES Techniques in Marine Environmental Sciences (TIMES),
708 vol. 36. ICES, Copenhagen.
709 Moore, M.N., Depledge, M.H., Readman, J.W., Leonard, P., 2004b. An integrated biomarker-based
710 strategy for ecotoxicological evaluation of risk in environmental management. Mutat. Res.
711 552, 247-268.

712 Moore, M.N., Allen, J.I., McVeigh, A., 2006a. Environmental prognostics: an integrated model
713 supporting lysosomal stress responses as predictive biomarkers of animal health status. Mar.
714 Environ. Res. 61, 278-304.
715 Moore, M.N., Allen, J.I., McVeigh, A., Shaw, J., 2006b. Lysosomal and autophagic reactions as
716 predictive indicators of environmental impact in aquatic animals. Autophagy 2, 217-220.
717 Moore, M.N., Viarengo, A., Donkin, P., Hawkins, A.J., 2007. Autophagic and lysosomal reactions
718 to stress in the hepatopancreas of blue mussels. Aquat. Toxicol. 84, 80-91.
719 Moore, M.N., Viarengo, A., Somerfield, P.J., Sforzini, S., 2012. Linking lysosomal biomarkers and
720 ecotoxicological effects at higher biological levels, in: Amiard-Triquet, C., Amiard, J.C.,
721 Rainbow, P.S. (Eds.), Ecological Biomarkers: Indicators of Ecotoxicological Effects. CRC
722 Press, Taylor & Francis Group, Boca Raton, FL, pp. 107-130.
723 Moore, M.N., Shaw, J.P., Ferrar Adams, D.R., Viarengo, A., 2015. Anti-oxidative cellular
724 protection effect of fasting-induced autophagy as a mechanism for hormesis. Mar. Environ.
725 Res. 107, 35-44.
726 Nasher, E., Heng, L.Y., Zakaria, Z., Surif, S., 2013. Concentrations and Sources of Polycyclic
727 Aromatic Hydrocarbons in the Seawater around Langkawi Island, Malaysia. Journal of
728 Chemistry. DOI: 10.1155/2013/975781.
729 Nott, J.A., Moore, M.N., Mavin, L.J. and Ryan, K.P., 1985. The fine structure of lysosomal
730 membranes and endoplasmic reticulum in the digestive gland of *Mytilus edulis* exposed to
731 anthracene and phenanthrene. Mar. Environ. Res. 17, 226-229.
732 Ohsaki, Y., Maeda, T., Fujimoto, T., 2005. Fixation and permeabilization protocol is critical for the
733 immunolabeling of lipid droplet proteins. Histochem. Cell Biol. 124, 445-452.
734 Orbea, A., Ortiz-Zarragoitia, M., Cajaraville, M.P., 2002. Interactive effects of benzo(a)pyrene and
735 cadmium and effects of di(2-ethylhexyl) phthalate on antioxidant and peroxisomal enzymes

736 and peroxisomal volume density in the digestive gland of mussel *Mytilus galloprovincialis*
737 Lmk. Biomarkers 7, 33-48.
738 Phillips, S.N., Muzaffar, N., Codlin, S., Korey, C.A., Taschner, P.E., de Voer, G., Mole, S.E.,
739 Pearce, D.A., 2006. Characterizing pathogenic processes in Batten disease: use of small
740 eukaryotic model systems. Biochim. Biophys. Acta 1762, 906–919.
741 Pipe, R.K. and Moore, M.N., 1985. Ultrastructural changes in the lysosomal-vacuolar system in
742 digestive cells of *Mytilus edulis* as a response to increased salinity. Mar. Biol. 87, 157-163.
743 Plant, A.L., Benson, D.M., Smith, L.C., 1985. Cellular uptake and intracellular localization of
744 benzo(a)pyrene by digital fluorescence imaging microscopy. J. Cell Biol. 100, 1295-1308.
745 Podechard, N., Le Ferrec, E., Rebillard, A., Fardel, O., Lecureur, V., 2009. NPC1 repression
746 contributes to lipid accumulation in human macrophages exposed to environmental aryl
747 hydrocarbons. Cardiovasc. Res. 82, 361-370.
748 Sedivy, R., 1999. Chaodynamic loss of complexity and self-similarity cancer. Med. Hypotheses 52,
749 271-274.
750 Sforzini, S., Moore, M.N., Boeri, M., Benfenati, E., Colombo, A.,Viarengo, A., 2014.
751 Immunofluorescence detection and localization of B[*a*]P and TCDD in earthworm tissues.
752 Chemosphere 107, 282-289.
753 Sforzini, S., Moore, M.N., Boeri, M., Bencivenga, M., Viarengo, A., 2015. Effects of PAHs and
754 dioxins on the earthworm *Eisenia andrei*: a multivariate approach for biomarker
755 interpretation. Environ. Pollut. 196, 60-71.
756 Sforzini, S., Moore, M.N., Mou, Z., Boeri, M., Banni, M., Viarengo, A., 2017. Mode of action of
757 Cr(VI) in immunocytes of earthworms: Implications for animal health. Ecotox. Environ. Saf.
758 138, 298-308.

759 Shannon, P., Markiel, A., Ozier, O., Baliga, N.S., Wang, J.T., Ramage, D., Amin, N., Schwikowski,
760 B., Ideker, T., 2003. Cytoscape: a software environment for integrated models of biomolecular
761 interaction networks. Genome Res. 13, 2498-2504.
762 Sinaei, M., Mashinchian, A., 2014. Polycyclic aromatic hydrocarbons in the coastal sea water, the
763 surface sediment and Mudskipper *Boleophthalmus dussumieri* from coastal areas of the
764 Persian Gulf: source investigation, composition pattern and spatial distribution. J. Environ.
765 Health Sci. Eng. 12(1):59. doi: 10.1186/2052-336X-12-59.
766 Soulard, A., Cohen, A., Hall, M.N., 2009. TOR signaling in invertebrates. Curr. Opin. Cell Biol. 21,
767 825-836.
768 Stegeman, J.J., 1985. Benzo[a]pyrene oxidation and microsomal enzyme activity in the mussel
769 (*Mytilus edulis*) and other bivalve mollusc species from the Western North Atlantic. Marine
770 Biology 89, 21-39.
771 Svendsen, C., Spurgeon, D.J., Hankard, P.K., Weeks, J.M., 2004. A review of lysosomal membrane
772 stability measured by neutral red retention: is it a workable earthworm biomarker? Ecotoxicol.
773 Environ. Saf. 57, 20-29.
774 U.S. EPA (Environmental Protection Agency), Appendix A to 40 CFR, Part 423-126 Priority
775 Pollutants, 2009.
776 Viarengo, A., 1989. Heavy metals in marine invertebrates: mechanisms of regulation and toxicity at
777 the cellular level. Rev. Aquat. Sci. 1, 295-317.
778 Viarengo, A., Nott, J.A., 1993. Mini-review: Mechanisms of heavy metal cation homeostasis in
779 marine invertebrates. Comp. Biochem. Physiol. C 104, 355-372.
780 Viarengo, A., Zanicchi, G., Moore, M.N., Orunesu, M., 1981. Accumulation and detoxication of
781 copper by the mussel Mytilus galloprovincialis Lam.: A study of the subcellular distribution in
782 the digestive gland cells. Aquat. Toxicol. 1, 147-157.

783 Viarengo, A., Lowe, D., Bolognesi, C., Fabbri, E., Koehler, A., 2007. The use of biomarkers in
784 biomonitoring: a 2-tier approach assessing the level of pollutant-induced stress syndrome in
785 sentinel organisms. Comp. Biochem. Physiol. C 146, 281-300.
786 Wang, X., Wang, W.-X., 2006. Bioaccumulation and transfer of benzo(a)pyrene in a simplified
787 marine food chain. Mar. Ecol. Prog. Ser. 312, 101-111.
788 Widdows, J., Donkin, P., Staff, F.J., Matthiessen, P., Law, R.J., Allen, Y.T., Thain, J.E., Allchin,
789 C.R., Jones, B.R., 2002. Measurement of stress effects (scope for growth) and contaminant
790 levels in mussels (*Mytilus edulis*) collected from the Irish Sea. Mar. Environ. Res. 53, 327-
791 356.
792 Winston, G.W., Moore, M.N., Kirchin, M.A., Soverchia, C., 1996. Production of reactive oxygen
793 species (ROS) by hemocytes from the marine mussel, *Mytilus edulis*. Comp. Biochem.
794 Physiol. 113C, 221-229.
795 Yang, Y., Liu, X., Zhang, X.X., Korenaga, T., 2001. Study on the dynamic complexation between
796 protein and PAHs by capillary electrophoresis. Analyt. Sciences 2001 17(ICAS2001): i1345-
797 i1349.
798

Table 1. Network model interactions and corresponding biomarker used for ascribing interaction strength.

Interaction	*Biomarker*
LYS-AUT	Lysosomal Membrane Stability (LMS)
LYS-OxSt	Lysosomal Membrane Stability (LMS)
AUT-LYS	Lysosomal -Cytoplasmic Volume Ratio (Lys/Cyt Vol)
AUT-OxSt	Lysosomal -Cytoplasmic Volume Ratio (Lys/Cyt Vol)
AUT-AUT	Lysosomal -Cytoplasmic Volume Ratio (Lys/Cyt Vol)
AUT-DNA dam	Lysosomal -Cytoplasmic Volume Ratio (Lys/Cyt Vol)
LIPID-LYS	Neutral Lipid (NL)
LIPID-AUT	Neutral Lipid (NL)
mTORC1-LYS	mTORC1 (mTOR)
mTORC1-AUT	mTORC1 (mTOR)
OxSt-AUT	Lipofuscin (LF)
OxSt-LYS	Lipofuscin (LF)
OxSt-LIPID	Lipofuscin (LF)
OxSt-mTOR	Lipofuscin (LF)
OxSt-DNA dam	Lipofuscin (LF)

LYS – Lysosomal function; AUT – Autophagy; OxSt – Oxidative stress; DNA dam – DNA damage; Lipid – Neutral lipid (triglyceride); mTORC1 – Mechanistic target of rapamycin complex 1.

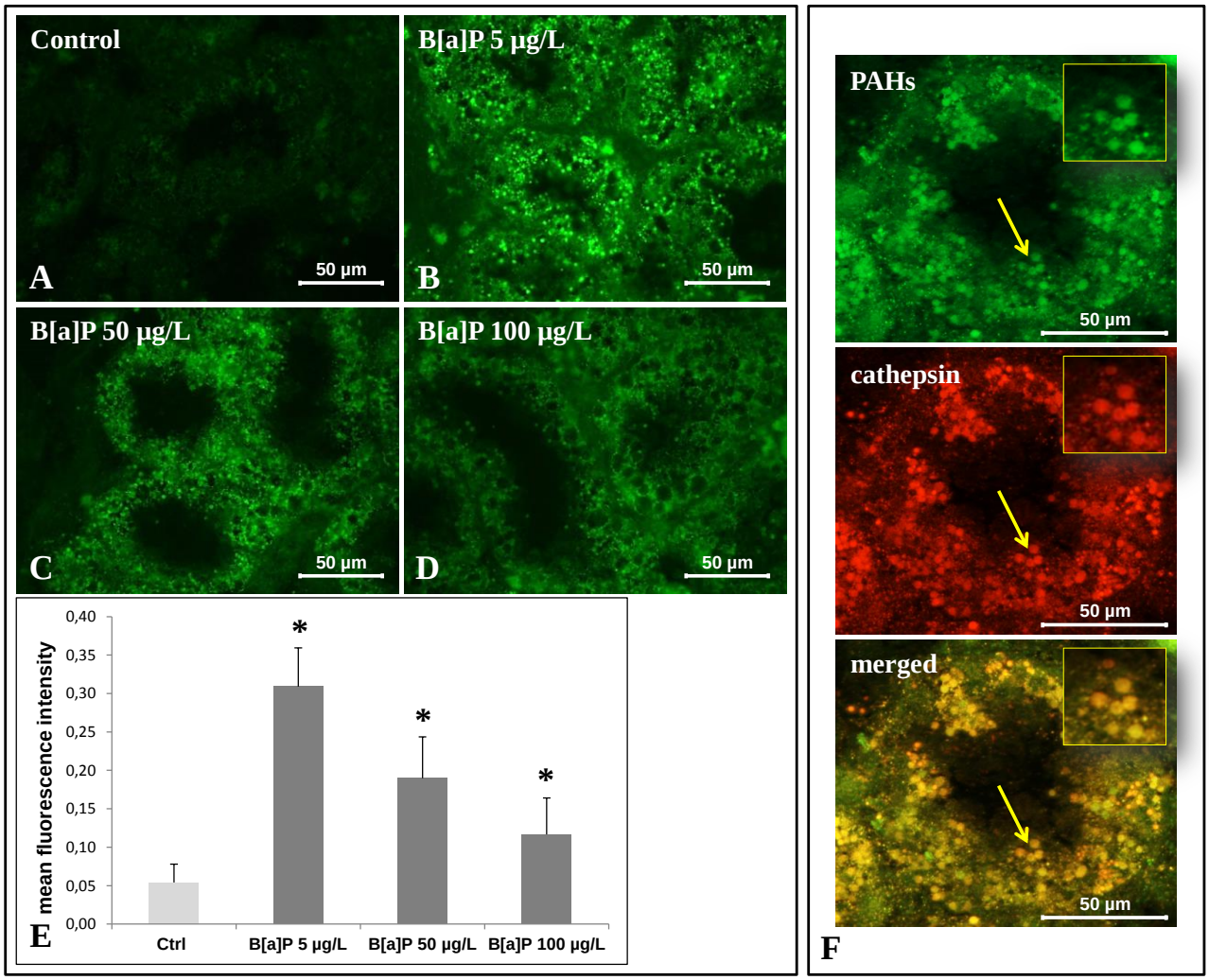
Control
A
50 µm
B[a]P 5 µg/L
B
50 µm
B[a]P 50 µg/L
C
50 µm
B[a]P 100 µg/L
D
50 µm
mean fluorescence intensity
0,40
0,35
0,30
0,25
0,20
0,15
0,10
0,05
0,00
*
*
*
Ctrl
B[a]P 5 µg/L
B[a]P 50 µg/L
B[a]P 100 µg/L
E
PAHs
50 µm
cathepsin
50 µm
merged
50 µm
F

Fig. 1.

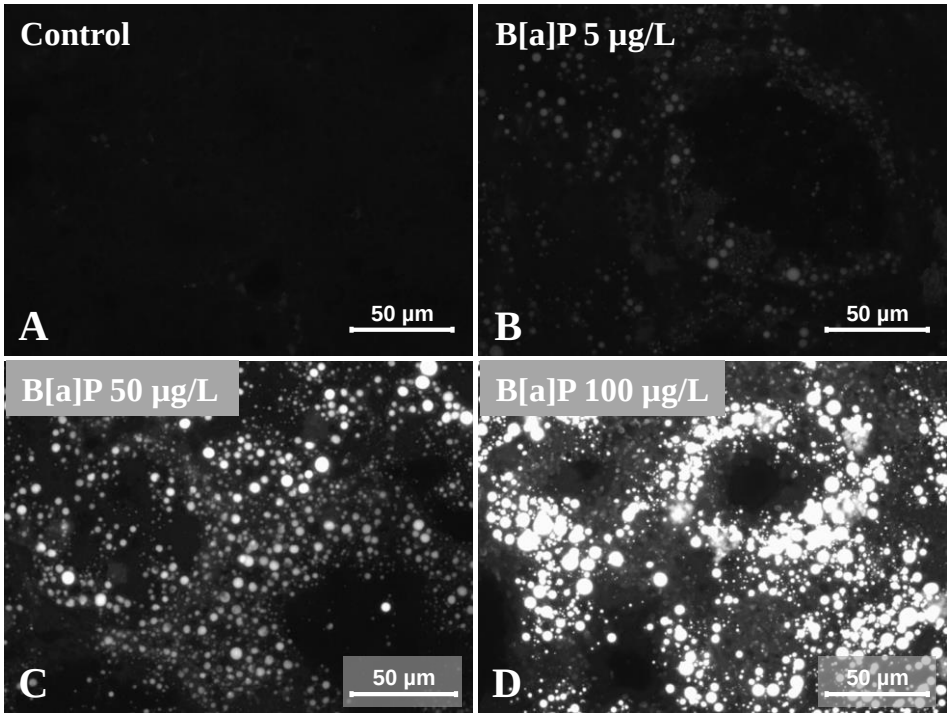

809

810 Fig. 2.

811

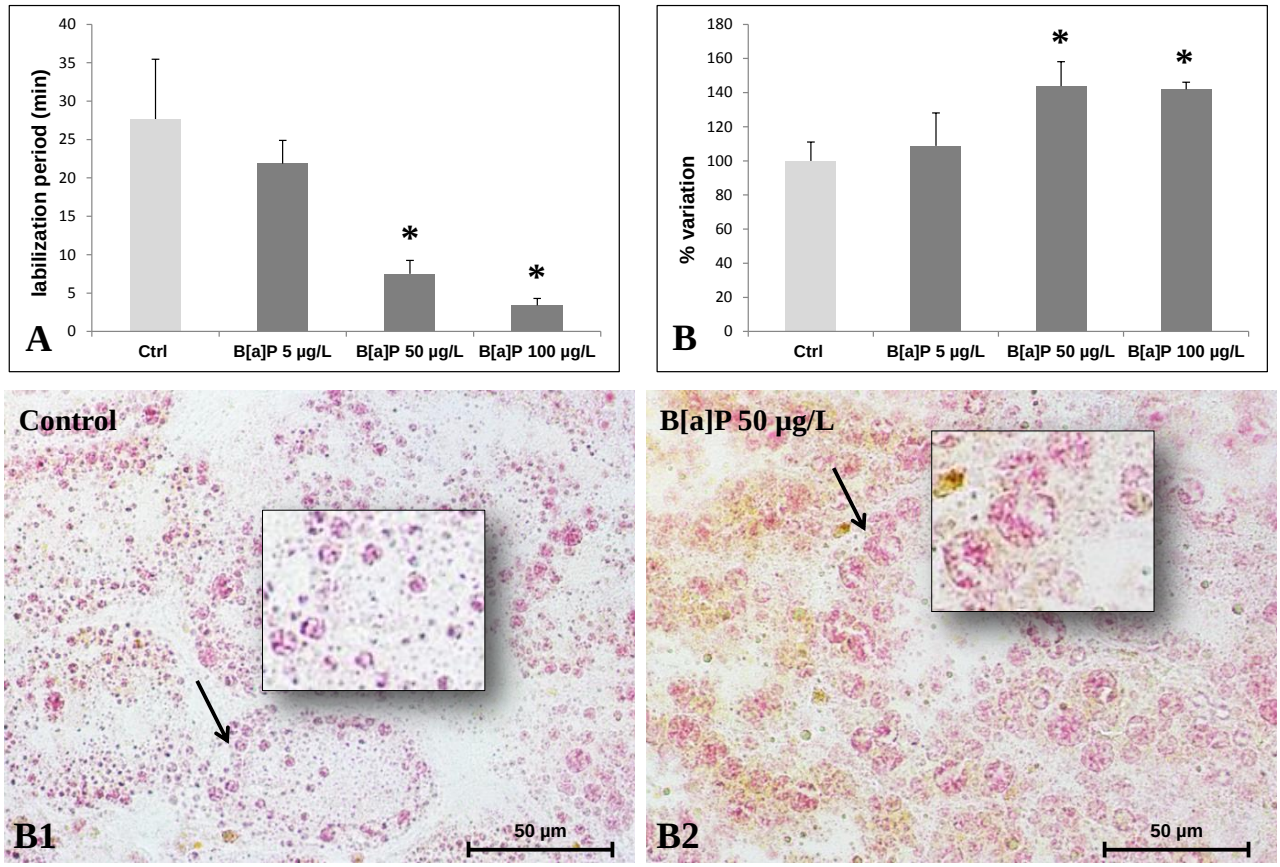

812

813 Fig. 3.

814

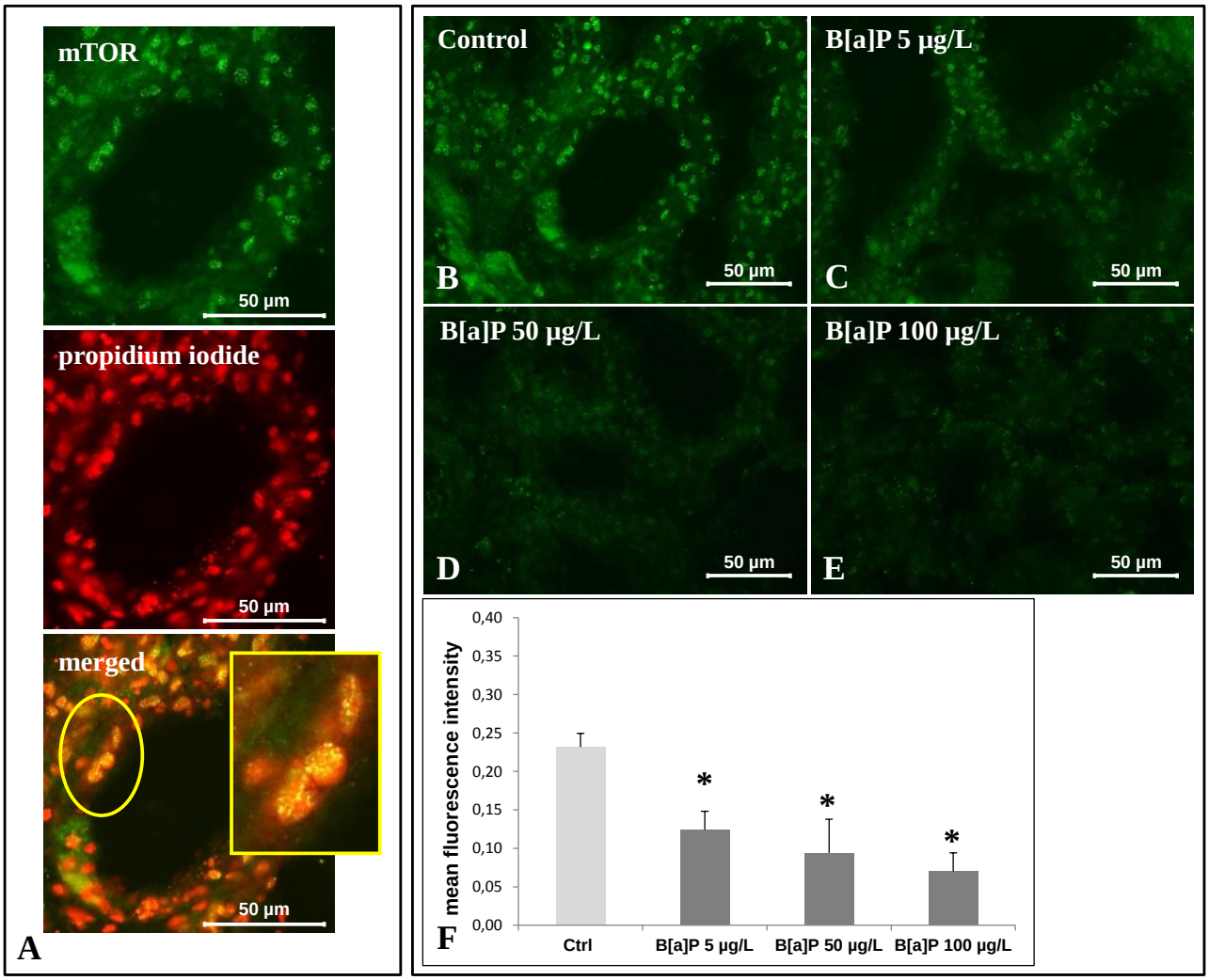
mTOR
50 µm
propidium iodide
50 µm
merged
50 µm
A
Control
B
50 µm
B[a]P 5 µg/L
C
50 µm
B[a]P 50 µg/L
D
50 µm
B[a]P 100 µg/L
E
50 µm
mean fluorescence intensity
0,40
0,35
0,30
0,25
0,20
0,15
0,10
0,05
0,00
*
*
*
Ctrl
B[a]P 5 µg/L
B[a]P 50 µg/L
B[a]P 100 µg/L
F

Fig. 4.

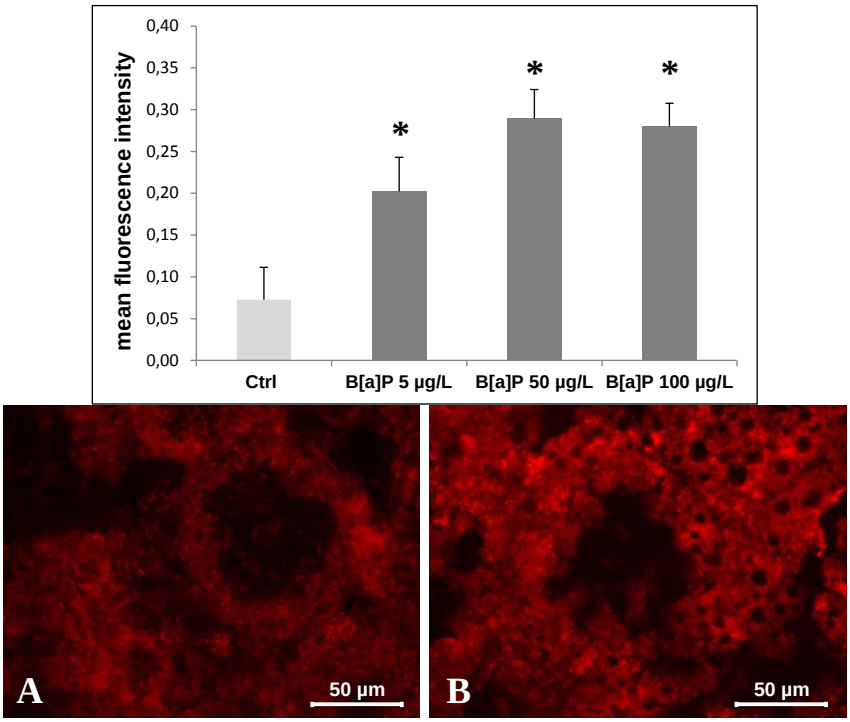

818

819 Fig. 5.

820

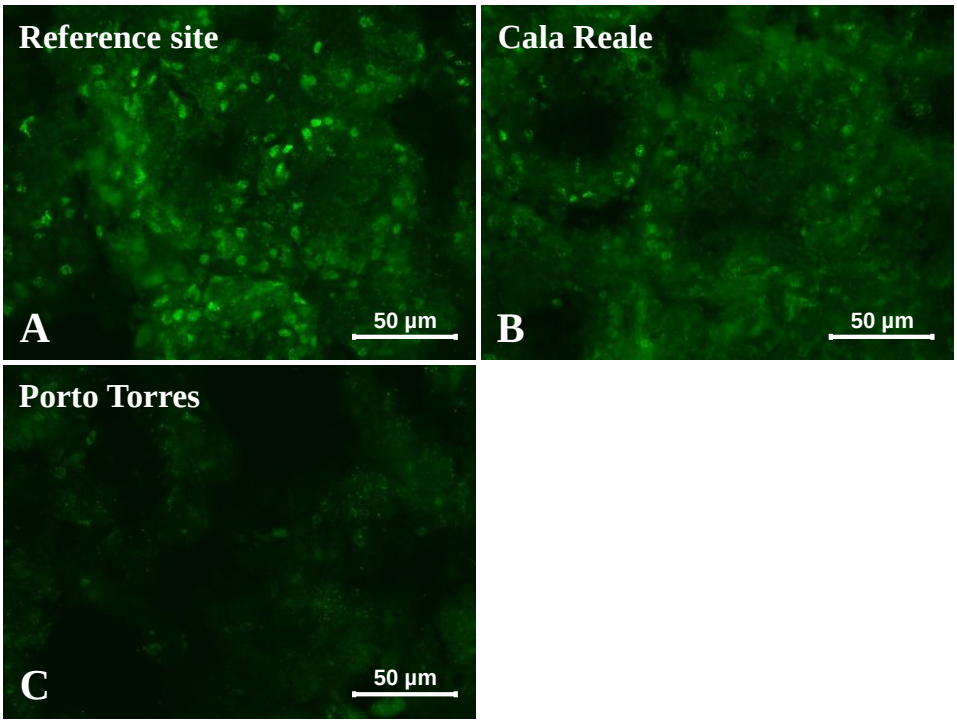

821

822 Fig. 6.

823

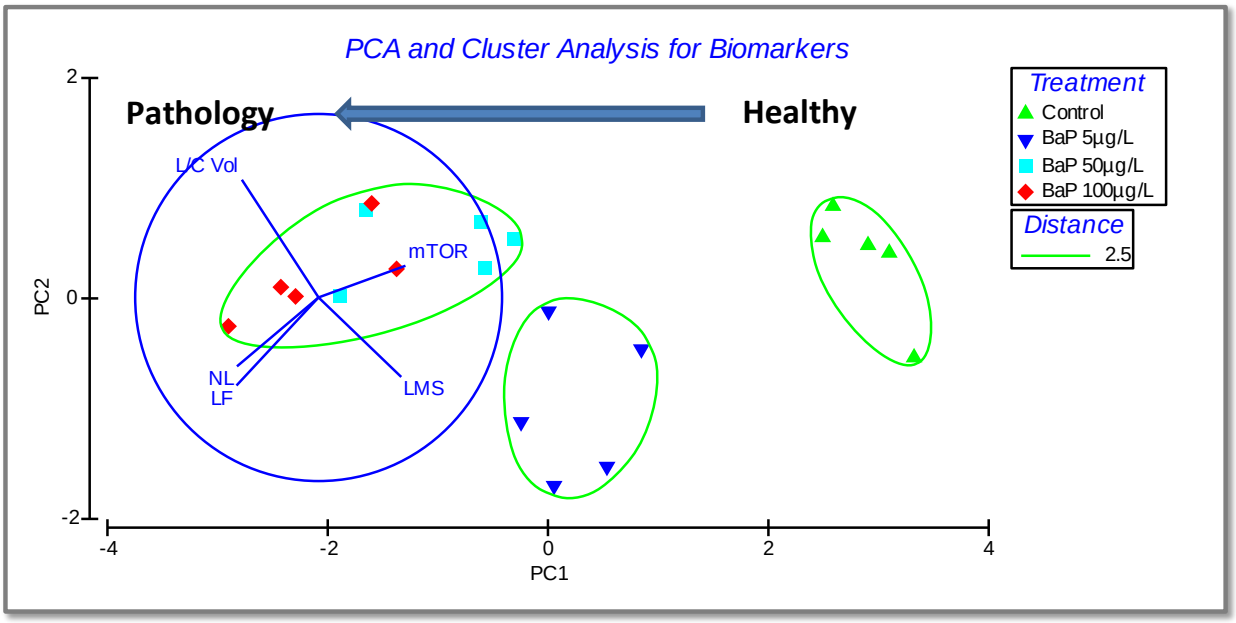

824

825 Fig. 7.

826

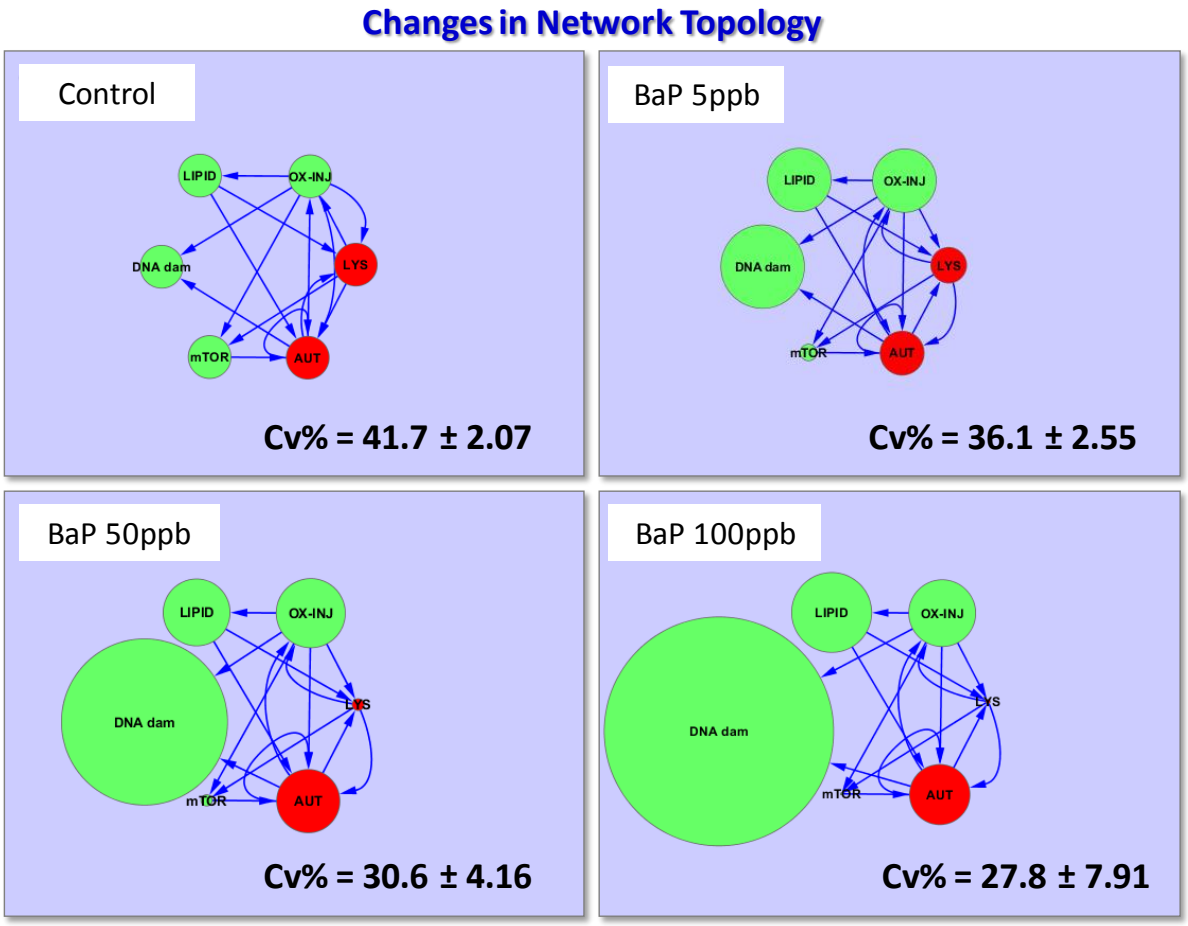

827

828 Fig. 8.

829

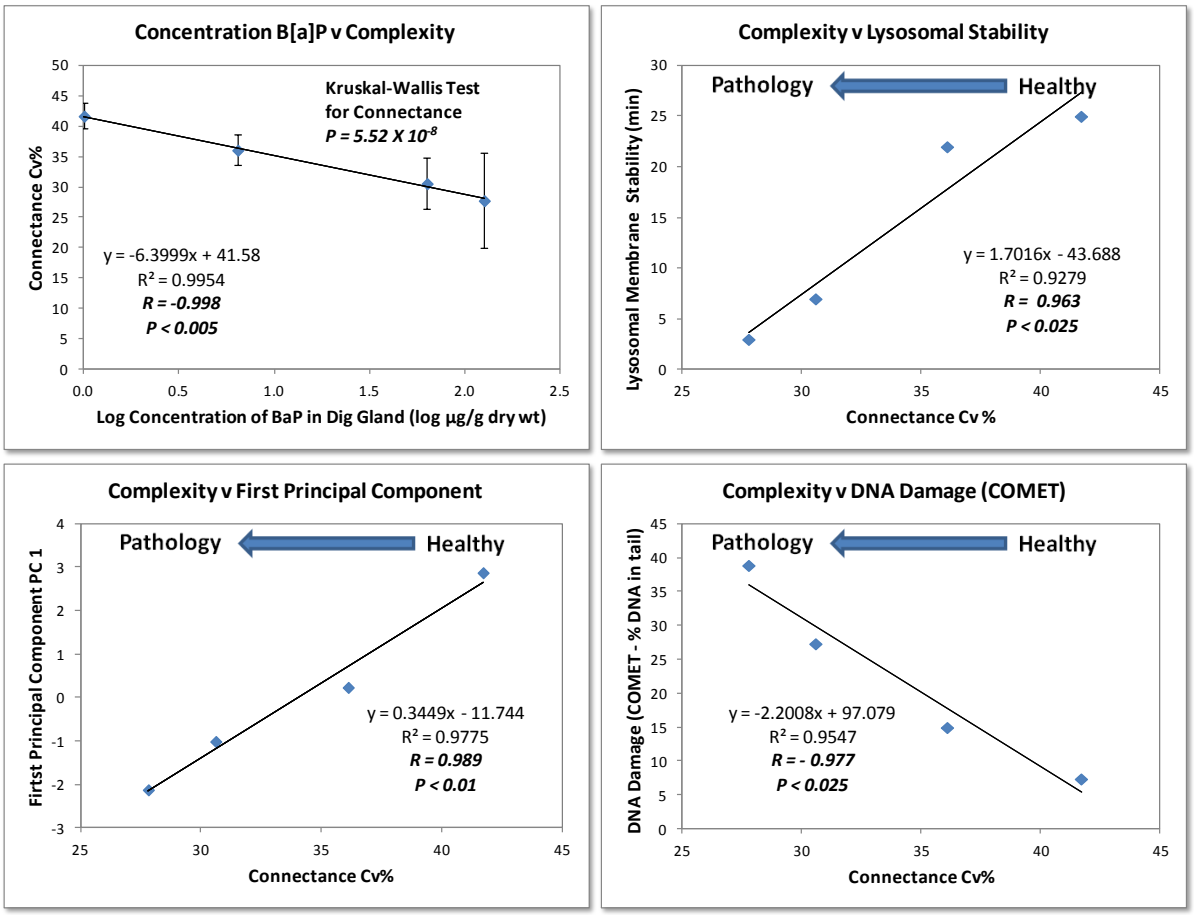

830

831 Fig. 9.

832

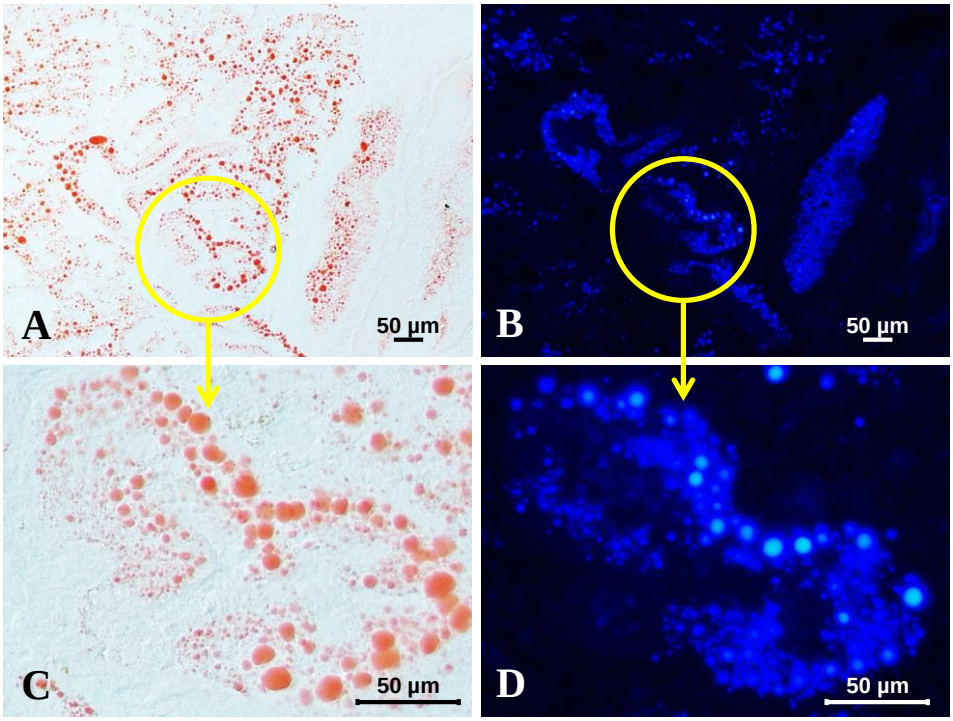

833

834 Fig. 10.

835

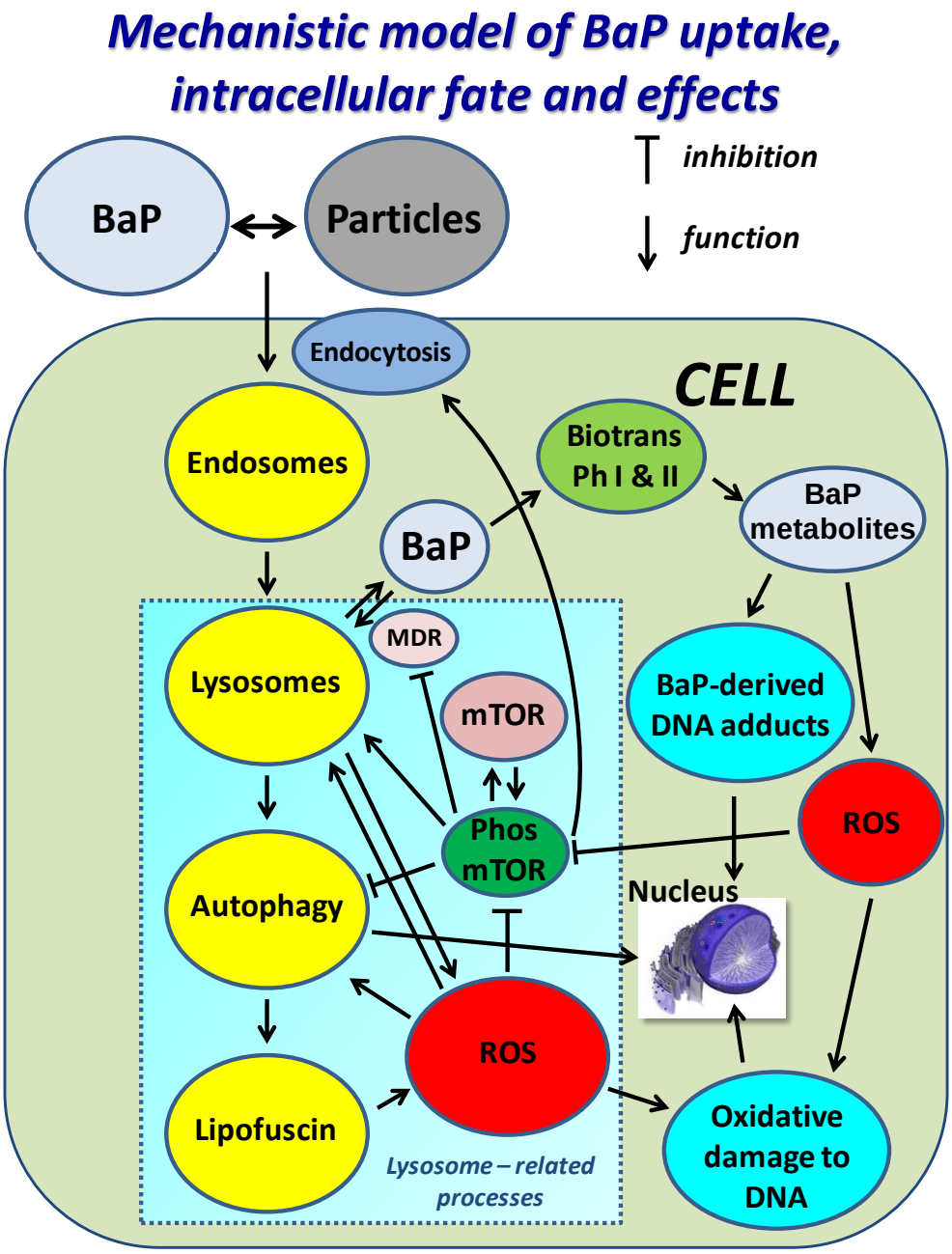

836

837

838 Fig 11.

839

Fig. 1. Anti-PAHs immunohistochemical staining (green: FITC conjugated secondary antibody) of digestive gland tissue sections from mussels exposed to different experimental conditions (A: Control; B: 5 μg/L B[*a*]P; C: 50 μg/L B[*a*]P; D: 100 μg/L B[*a*]P). E) Quantitative fluorescence analysis of anti-PAHs immunoreaction. Data are mean ± SD of at least five replicates; * = $p < 0.05$ (Mann-Whitney *U*-test). F) Double immunohistochemical staining of digestive glands from mussels exposed to 5 μg/L B[*a*]P with anti-PAHs and -cathepsin D antibodies (separate colour images for PAHs (FITC, green) and cathepsin D (DyLight594, red) immunoreactivity were merged into a composite image, whereby the colocalization of both antigens in lysosomes of B[*a*]P exposed mussels was revealed through the coincidence of the two labels resulting in a yellow colour -see arrows and insets).

Fig. 2. Cryostat unstained sections of digestive glands from mussels exposed to different experimental conditions (A: Control; B: 5 μg/L B[*a*]P; C: 50 μg/L B[*a*]P; D: 100 μg/L B[*a*]P) examined with UV excitation: white-blue fluorescent deposits, in form of droplets, were evident particularly at the higher B[a]P concentrations (C, D) (grayscale images).

Fig. 3. Lysosomal biomarker responses in digestive gland of mussels exposed to B[*a*]P (5, 50, 100 μg/L). A) Lysosomal membrane stability (cytochemical assay based on acid labilization characteristics of latent hydrolase β-*N*-acetylhexosaminidase); B) lysosomal/cytoplasmic volume ratio (lysosomes reacted for the lysosomal enzyme β-*N*-acetylhexosaminidase: when compared to controls (B1), in mussels exposed to B[*a*]P an enlargement of autolysosomes was observed (B2), see arrows and insets). Data represent the mean ± SD of at least five replicates. * indicates statistically significant differences ($p < 0.05$ Mann-Whitney *U*-test).

Fig. 4. Anti-mTOR (phospho S2448) immunohistochemical staining (green: Chromeo conjugated secondary antibody) of digestive gland tissue sections from mussels exposed to different experimental conditions. (A; B) Control (in A separate colour images for mTOR immunoreactivity (Chromeo, green) and the nuclear counterstain propidium iodide (red) were merged into a composite image, whereby the yellow colour highlights the localization of mTOR in perinuclear region of the tubule epithelial cells); C) 5 μg/L B[*a*]P; D) 50 μg/L B[*a*]P; E) 100 μg/L B[*a*]P). (F) Quantitative fluorescence analysis of anti-mTOR immunoreaction. Data are mean ± SD of at least five replicates; * = $p < 0.05$ (Mann-Whitney *U*-test).

Fig. 5. Quantitative fluorescence analysis of anti-mTOR immunoreaction of digestive gland tissue sections from mussels exposed to B[*a*]P. Data represent the mean ± SD of at least five replicates. * indicates statistically significant differences ($p < 0.05$ Mann-Whitney *U*-test). Representative images of tissue sections of controls (A) and 50 μg/L B[*a*]P exposed mussels (B) (red: DyLight594 conjugated secondary antibody).

Fig. 6. Anti-mTOR (phospho S2448) immunohistochemical staining (green: Chromeo conjugated secondary antibody) of digestive gland tissue sections from mussels caged at three sites along the Sardinian coast. A) Reference site (Porto Mannu li Fornelli); B) Cala Reale; D) Porto Torres.

Fig. 7. Principal component (PCA) and cluster analysis of the biomarker data not including DNA damage. Vectors indicate the directionality of specific biomarkers.

Fig. 8. Interaction network models based on the physiological and pathological processes represented by the biomarker investigations in mussel digestive cells. Processes represented include lysosomal function, autophagy, mTORC1 signalling, lysosomal lipid accumulation, oxidative injury

889 and DNA damage. Node sizes are based on the proportional change in the biomarker representing
890 the process (see Table 1). System complexity (Connectance Cv% ± 95% CL, n = 5) is shown for
891 each treatment.
892
893 Fig. 9. Statistical modelling for system complexity versus B[*a*]P concentration (showing ± 95%CL
894 for Cv%, n = 5), lysosomal stability, first principal component and DNA damage (COMET).
895
896 Fig. 10. Representative images of cryostat serial sections of digestive glands from mussels exposed
897 to B[*a*]P 100 µg/L (A, C) stained with Oil-Red O for the evaluation of lysosomal neutral lipid
898 content and (B, D) unstained and analysed with UV excitation, showing that the distribution of the
899 B[a]P fluorescent droplets in the digestive gland cells corresponds to that of the neutral lipid
900 containing vesicles.
901
902 Fig 11. Diagrammatic representation of an explanatory mechanistic framework for the
903 interconnected cellular reactions to B[*a*]P based on the biomarker data, network modelling and
904 other published sources in the scientific literature. ROS - reactive oxygen species; Phos mTOR -
905 active phosphorylated form of mTORC1 cell signalling system; mTOR - inactive dephosphorylated
906 form of mTORC1; MDR – Pgp40 multidrug transporter; BIOTRANS Ph I & II - Phase I and II
907 biotransformation system (Canova et al., 1998).
908

-The autophagic process in digestive gland of B[*a*]P exposed mussels was investigated.

-B[a]P accumulated in lysosomes/enlarged lipid-rich lysosomes of digestive cells.

-At higher doses B[*a*]P overstimulated the autophagy and increased cell catabolism.

-B[*a*]P-induced dephosphorylation of mTOR may explain the observed pathological effects.

-Network connectedness showed that pathology results in a loss of system complexity.

Supplementary Information

Western blot analysis

Digestive glands were homogenised with NP-40 buffer (150mM sodium chloride, 1% Triton, 50mMTris, pH 8.0) containing 1/100 of protease inhibitor cocktail (Sigma-Aldrich) and centrifuged at 1000 rcf for 5 min at 4°C. Pellets were resuspended in the NP-40 buffer and 10 µg of proteins were loaded on a Mini-Protean TGX 4-15% gel (Bio-Rad Laboratories S.r.l) for SDS-PAGE, under reducing conditions. Following electrophoresis, the proteins were transferred onto PVDF membranes in transfer buffer. The membranes were blocked with 5% BSA solution at 4 °C for 1 h. The blots were incubated overnight at 4˚C with the primary antibody (anti m-TOR (phospho S2448) antibody, Abcam, ab84400) at 1 ug/ml, followed by incubating with a 1:5000-diluted HRP-conjugated goat anti-rabbit secondary antibody (Bio-Rad Laboratories S.r.l.) for 90 minutes, and then visualized by Clarity™ ECL detection kit. (Bio-Rad Laboratories S.r.l.).

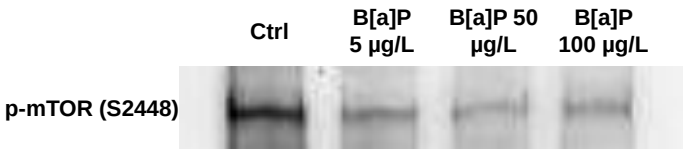

Fig. S1. Western blot analysis of p-mTOR (S2448) protein indicating that B[*a*]P induces a dephosphorylation of the protein. Protein bands shown are representative of 3 independent experiments with similar results.

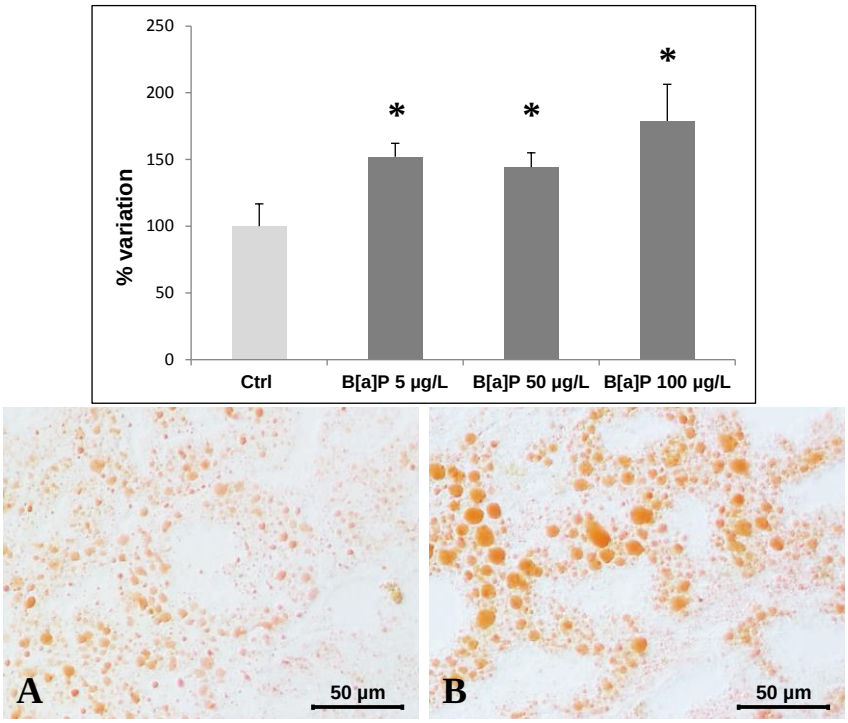

934

935 Fig. S2. Lysosomal neutral lipid content in the digestive gland cells of mussels exposed to B[*a*]P (5,
936 50, 100 µg/L). Data, expressed as percent change with respect to control values, represent the mean
937 ± SD of at least five replicates. * indicates statistically significant differences ($p < 0.05$ Mann–
938 Whitney *U*-test). Representative images of tissue sections from control (A) and B[*a*]P-exposed
939 mussels (B) (100 µg/L).